Earth and Planetary Science Letters 325-326 (2012) 76–84

Contents lists available at SciVerse ScienceDirect

Earth and Planetary Science Letters

journal homepage: www.elsevier.com/locate/epsl

Relationship between topography, rates of extension and mantle dynamics in the actively-extending Italian Apennines

J.P. Faure Walker [a], G.P. Roberts [a], P.A. Cowie [b], I. Papanikolaou [a], A.M. Michetti [c], P. Sammonds [a], M. Wilkinson [d], K.J.W. McCaffrey [d], R.J. Phillips [e]

[a] Research School of Earth Sciences, UCL/Birkbeck, Gower Street, London, WC1E 6BT, UK
[b] Institute of Geography School of GeoSciences, University of Edinburgh, Drummond Street, Edinburgh, EH8 9XP, UK
[c] Dipartimento di Scienza e Alta Tecnologia, Università dell'Insubria, Via Valleggio 11, 22100, Como, Italy
[d] Department of Earth Sciences, University of Durham, Durham DH1 3LE, UK
[e] School of Earth and Environment, University of Leeds, Leeds, LS2 9JT, UK

ARTICLE INFO

Article history:
Received 11 February 2011
Received in revised form 19 January 2012
Accepted 23 January 2012
Available online xxxx

Editor: Y. Ricard

Keywords:
active normal fault
strain
Italy
late Pleistocene–Holocene
topography
extension

ABSTRACT

To investigate the mechanism driving active extension in the central and southern Italian Apennines and the geography of seismic hazard, we compare spatial variations in upper crustal strain-rate measured across exposed fault scarps since 15 ± 3 ka with data on cumulative upper-crustal strain and topographic elevation, and free-air gravity, P-wave tomography and SKS splitting delay times that are a proxy for strain in the mantle. High extensional strain-rates across the Apennines since 15 ± 3 ka (0.4–3.1 mm/yr along 90 km transects) occur in two areas (Lazio-Abruzzo; SE Campania and Basilicata) where values for finite extensional strains that have developed since 2–3 Ma are highest (2–7 km cumulative throw), and where mean elevation in 5×90 km NE–SW boxes is >600 m; the intervening area (NW Campania and Molise) with <600 m mean elevation in 5×90 km boxes has extension-rates <0.4 mm/yr and lower values for finite extensional strains (<2 km cumulative throw). These two areas with high upper-crustal strain-rates overlie mantle that has relatively-long spatially-interpolated SKS delay times (1.2–1.8 s) indicating relatively-high mantle strains and free-air gravity values (140–160 mGals); the intervening area of lower extension-rate has shorter spatially-interpolated SKS delay times (0.8–1.2 s) and lower free-air gravity values (120 mGals). The two areas with high upper crustal strain-rates and strain, mean elevation, and mantle strain, coincide with the northern and southern edges of a slab window in the Tyrrhenian–Apennines subducting plate that has been inferred from published P-wave tomography. Together these correlations suggest that dynamic support of the topography by mantle flow through the slab window may control the present day upper crustal strain-rate field in the Apennines and the geography of seismic hazard in the region.

1. Introduction

Northeast–southwest active extension accommodated by normal faults in the Apennines, localised on the crest of ~700 km long, <90 km wide, NW–SE trending topographic bulge of the Apennine mountains, occurs in previously shortened continental crust positioned within the zone of convergence between the Eurasian and African Plates (Anderson and Jackson, 1987; Doglioni, 1995; Jolivet et al., 1998; Mazzoli and Helman, 1994) (Fig. 1). Debate continues concerning the mechanism driving this extension. One view is that the extension is driven by edge effects, that is, the forces resulting from motions that occur along the neighbouring plate boundaries; these forces are a product of the relative motions of rigid plates rotating about Euler poles (D'Agostino et al., 2008). Another view is that extension is influenced by uplift within the Apennines, where "mantle upwelling beneath the central Apennines has been the dominant geodynamical process during the Quaternary, controlling both the geomorphological evolution and the distribution of active deformation" (D'Agostino et al., 2001). This second viewpoint has emerged because admittance analysis of gravity data shows that the topographic relief at wavelengths longer than 150 km is supported dynamically by mantle convection, suggesting that the topographic bulge, and the active normal faults, have formed due to upwelling mantle beneath the Apennines (D'Agostino et al., 2001). Although a qualitative link between mantle upwelling and the location of extension has been described (D'Agostino et al., 2001), this study did not quantify the relationship between strain-rates and finite strains in the upper crust, topography and geophysical evidence for flow/strain in the mantle.

We investigate the proposed relationship between uplift, topography, mantle upwelling, and strain and strain-rates in the upper crust. If topography is a proxy for uplift produced by mantle upwelling (whilst taking lithology and erosion properly into account), and the upwelling influences the extension (as suggested by D'Agostino et al. (2001)), we would expect spatial variation in upper-crustal strain-rates to correlate with spatial variation in topography. We have measured the spatial variation in upper-crustal strain-rates

0012-821X/$ – see front matter © 2012 Elsevier B.V. All rights reserved.
doi:10.1016/j.epsl.2012.01.028

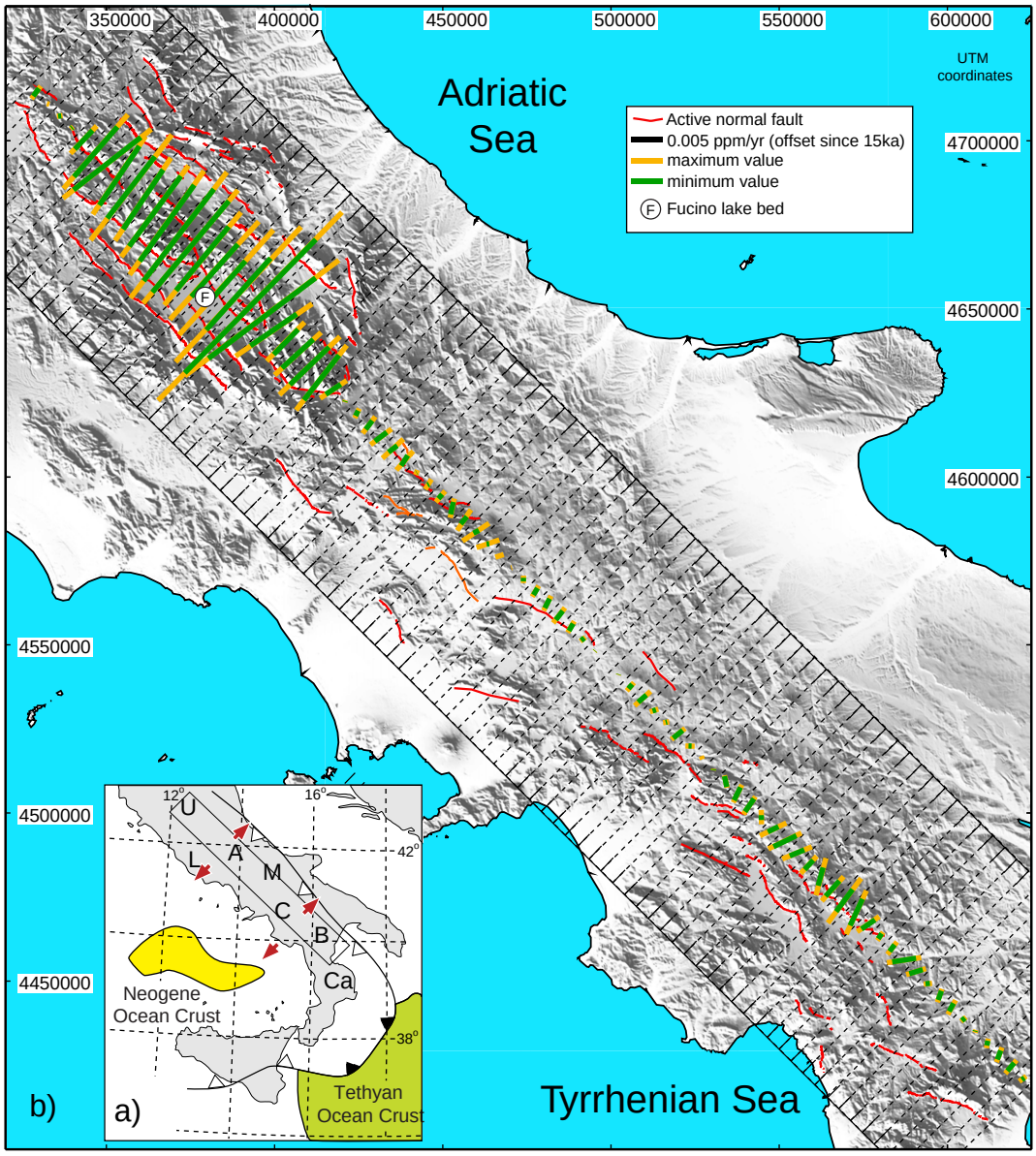

Fig. 1. Map showing the spatial variation in principal horizontal strain calculated in 5 × 90 km boxes (dashed lines) traversing the Italian Apennines, derived from the directions and magnitudes of faulted-offsets since 15 ± 3 ka of landforms dating from the last glacial maximum. (a) Location of study area indicated in the inset box. (b) SRTM DEM with strain-rate bars overlain with a UTM grid. U = Umbria, L = Lazio, A = Abruzzo, M = Molise, C = Campania, B = Basilicata, Ca = Calabria.

produced by long-term (since 15 ± 3 ka) slip-rates on active normal faults in the central and southern Apennines and compared these with spatial variations in mean elevation (Figs. 1 and 2). The strain-rates have been calculated by combining (1) slip-rate data derived from faulted offsets of land surfaces and deposits formed during the last glacial maximum, and (2) slip-directions measured from outcropping striated faults. These combined data allow determination of strain-rate tensors for the time period since 15 ± 3 ka. We also examine the total offsets that have accumulated across the faults during the Quaternary and perhaps since 2–3 Ma. The mean elevations have been sampled from SRTM data. We show that upper-crustal strain-rates and finite strain vary along the length of the central and southern Apennines, showing a positive correlation with mean elevation. We review published measurements influenced by the mantle such as free-air gravity, SKS splitting delay times and P-wave tomography and compare them with our measurements of the upper crust (Fig. 3). We find spatial correlations between independent datasets (Fig. 4), implying that uplift related to mantle flow influences extension in the upper crust. We use this to discuss continental extension in the Apennines and the geography of seismic hazard in the region.

2. Extension, uplift and seismicity of the Apennines

Extension in the central and southern Apennines, associated with moderate/large magnitude earthquakes such as the 6th April 2009 M 6.3 L'Aquila earthquake (307 deaths, 80,000 homeless (Anzidei et al., 2009; Atzori et al., 1996; Walters et al., 2009)), commenced after thrusting in this region ceased during the Pliocene (Cavinato and De Celles, 1999) (Fig. 1). Importantly for this paper, extension has been accompanied by uplift relative to sea-level, which increases in magnitude away from the Adriatic and Tyrrhenian coasts inwards towards the Apennine Mountains (D'Agostino et al., 2001).

The present-day/recent uplift-rates in the Apennines have been measured through repeated geodetic levelling of road networks during

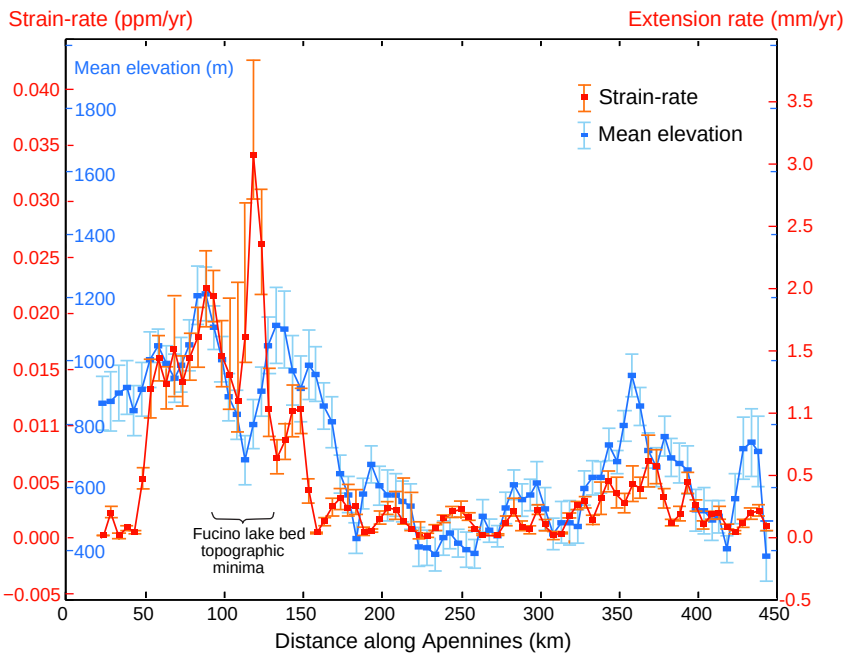

Fig. 2. Graph showing spatial variation in strain-rate, extension rate and mean elevation along the strike of the Apennines. Extension rates are calculated from strains within the 5×90 km boxes shown in Fig. 1. Topography has been sampled from the SRTM 90 m DEM. Transect is through the strain-rate bars in Fig. 1.

the periods 1870–1905, 1943–1959 and 1980–2003 (D'Anastasio et al., 2006). This re-levelling reveals uplift rates in the range of 0–0.5 mm/yr close to the coasts increasing to 1.0–1.5 mm/yr in the centre of the topographic bulge of the Apennines. This bulging mimics the topographic variations in the Italian peninsula with low elevation coastal plains separated by the high elevations (up to 2900 m) of the Apennines.

Regional bulging has been active during the Quaternary and perhaps earlier, based on the elevations of marine terraces and Holocene coastal notches (Bordoni and Valensise, 1998). For example, near the Tyrrhenian coast, remnant Neogene–Pleistocene marine deposits increase in elevation inland towards the northeast (Marinelli et al., 1993). Early Pleistocene shorelines inland of Rome, exposed for almost 100 km along NW–SE strike, have been uplifted by 200–400 m by a large-wavelength regional uplift (Ambrosetti et al., 1982); strontium isotope analyses of palaeoshoreline deposits constrain the age of the youngest at 1.65–1.5 Ma, giving estimated uplift rates of 0.17–0.34 ± 0.03 mm/yr (Mancini et al., 2007). Further inland in the Apennine mountains, remnants of a flat palaeolandscape formed by erosional processes close to sea-level during the Pliocene have been identified at high elevations (1350–1500 m), indicating uplift of over 1000 m since the Pliocene (Galadini et al., 2003). An uplift rate of 2.5 mm/yr over the last 1.6 Ma has been estimated using geological units and sedimentation rates for this portion of the central Apennines (Ghisetti and Vezzani, 1999). Quaternary uplift rates decrease NE towards the Adriatic coast evidenced by the northeast trending parallel drainage network (Demangeot, 1965; Dramis, 1992; Dufaure et al., 1989; Mazzanti and Trevisan, 1978), and northeast dipping Pleistocene marine-deltaic deposits (Cantalamessa et al., 1986; Ori et al., 1993). Uplift of the Apennines has produced high erosion rates recorded by the high volume of Quaternary sediments in the northern Tyrrhenian Sea (Zattin et al., 2000). This regional uplift occurs at rates that are high enough to uplift both the footwalls and the hangingwalls of the active normal faults relative to sea-level. For example, the occurrence of a marine ostracod assemblage in the Upper Pliocene to Lower Pleistocene deposits in the hangingwall of the Rieti fault (R on Fig. 3) indicates that brackish/marine marshes deposited close to sea-level have been uplifted by c. 400 m after the Early Pleistocene (Gliozzi and Mazzini, 1998). A similar pattern of uplift exists in the Southern Apennines, evidenced by marine terraces and coastal notches, basal unconformities, shallow-marine regression surfaces, and continental erosional surfaces (Ferranti and Oldow, 2005).

It has been suggested that the timing of the uplift of the Apennines coincides with or post-dates the change from shortening to extension ruling out crustal thickening as the dominant cause (D'Agostino et al., 2001), although Mele et al. (2006), who identify P-to-S phases converted at the Moho, show that the crustal thickness may peak at 39–47 km under the high topography of the Apennines, and suggest that topography could be supported, at least in part, by a crustal root. However, values for free-air gravity, together with study of the admittance associated with these data, suggest that the topography is dynamically supported by mantle convection, specifically mantle rising beneath the main topographic bulge of the Apennines (D'Agostino et al., 2001). These authors point out that other independent lines of evidence support the contention that mantle processes contribute to the regional uplift in the Apennines, such as (i) attenuated upper mantle seismic velocities beneath the Apennines (Mele et al., 1996,1997), (ii) Quaternary mantle-derived magmatism (Beccaluva et al., 1989; Serri et al., 1993), and (iii) mantle-derived helium in ground waters and natural gases (Hooker et al., 1985; Italiano et al., 2000). The area is underlain by a window through a subducted slab imaged by P-Wave tomography (Rosenbaum et al., 2008, Fig. 3i). SKS splitting delay times vary along the strike of the Apennines and have been discussed in terms of mantle strain associated with flow through the slab window (Lucente and Margheriti, 2008; Lucente et al., 2006, Fig. 3h).

Extension in the upper crust in the central and southern Apennines is accommodated by active normal faults (Fig. 1). These major faults have lengths of 20–30 km, throws that have accumulated in the Quaternary and perhaps since 2–3 Ma of 0.75–2.0 km (see Roberts and Michetti (2004) for discussion of this timing), and throw-rates averaged since 15 ± 3 ka of 0.3–2.0 mm/yr measured from offsets of sediments and landforms that were produced during the last glacial maximum (Faure Walker, 2010; Faure Walker et al., 2010; Faure Walker et al., 2009; Galadini and Galli, 2000; Morewood and Roberts, 2000; Papanikolaou and Roberts, 2007; Papanikolaou et al., 2005; Pizzi et al., 2002; Roberts and Michetti, 2004). Some of these authors also measured the kinematics of the

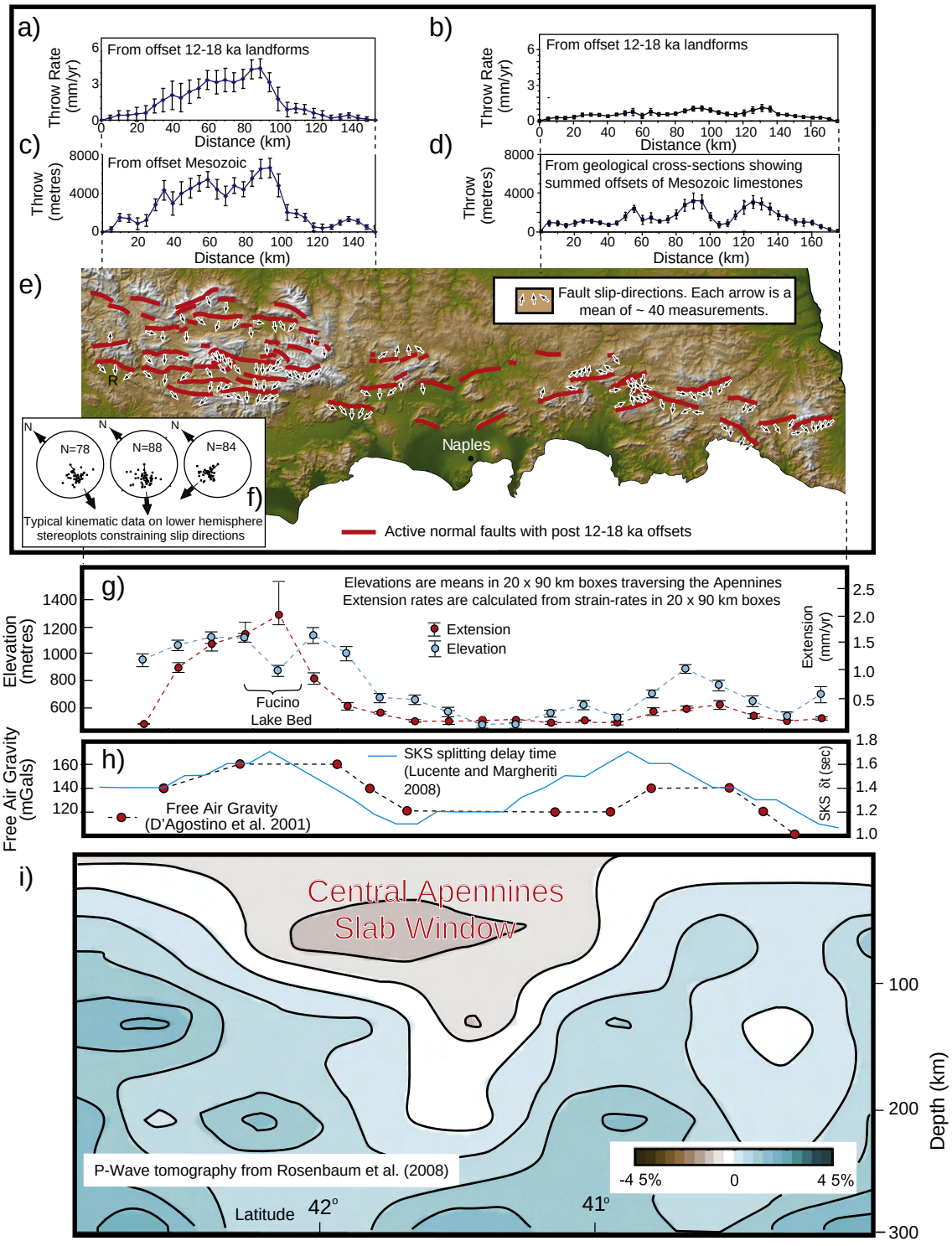

Fig. 3. Spatial relationships between throw-rates since 15 ± 3 ka summed across strike (a, b), throws in the Quaternary and perhaps since 2–3 Ma summed across strike (c, d; from Roberts and Michetti (2004) and Papanikolaou and Roberts (2007), SRTM topography and a fault map (e), post 15 ± 3 ka strain-rates calculated in 20 × 90 km boxes and topography (g), free-air gravity and SKS splitting delay times (h), and P-wave tomography (i). (e) and (f) summarise kinematic data for the active faults derived from striated and corrugated fault planes (from Faure Walker (2010), Faure Walker et al. (2010), Papanikolaou and Roberts (2007), Papanikolaou et al. (2005), Roberts and Michetti (2004)). All panels are at the same scale and are aligned with respect to distance along the strike of the Apennines and data have been projected onto a transect through the strain-rate bars in Fig. 1. Free-air gravity values are from a profile from Longitude 42.3505°, Latitude 12.5943° to Longitude 39.6680°, Latitude 16.3674° across Fig. 4b of D'Agostino et al. (2001). SKS splitting delay times in (h) were sampled along a traverse from Longitude 42.5588°, Latitude 12.8093° to Longitude 40.08342°, Latitude 16.5267° across Fig. 1 of Lucente and Margheriti (2008). The tomographic profile in (j) is re-drawn from Fig. 4 of Rosenbaum et al. (2008), sampled from Longitude 42.6171°, Latitude 12.7399° to Longitude 39.5674°, Latitude 16.2729°, but has been projected onto a line from Longitude 42.6653°, Latitude 12.8093° to Longitude 40.0834°, Latitude 16.5267° to show how the slab window relates to the other datasets. R in (e) locates the Rieti Basin.

faults, recorded by striated and corrugated fault planes exposed along the post 15 ± 3 ka scarps (Fig. 3e and f). These combined data for the active normal faults allow strain-rate tensors to be calculated (Faure Walker, 2010; Faure Walker et al., 2010, see below). Geological cross-sections constrain faulted offsets of Mesozoic strata in the upper crust across the active normal faults (Faure Walker, 2010; Papanikolaou

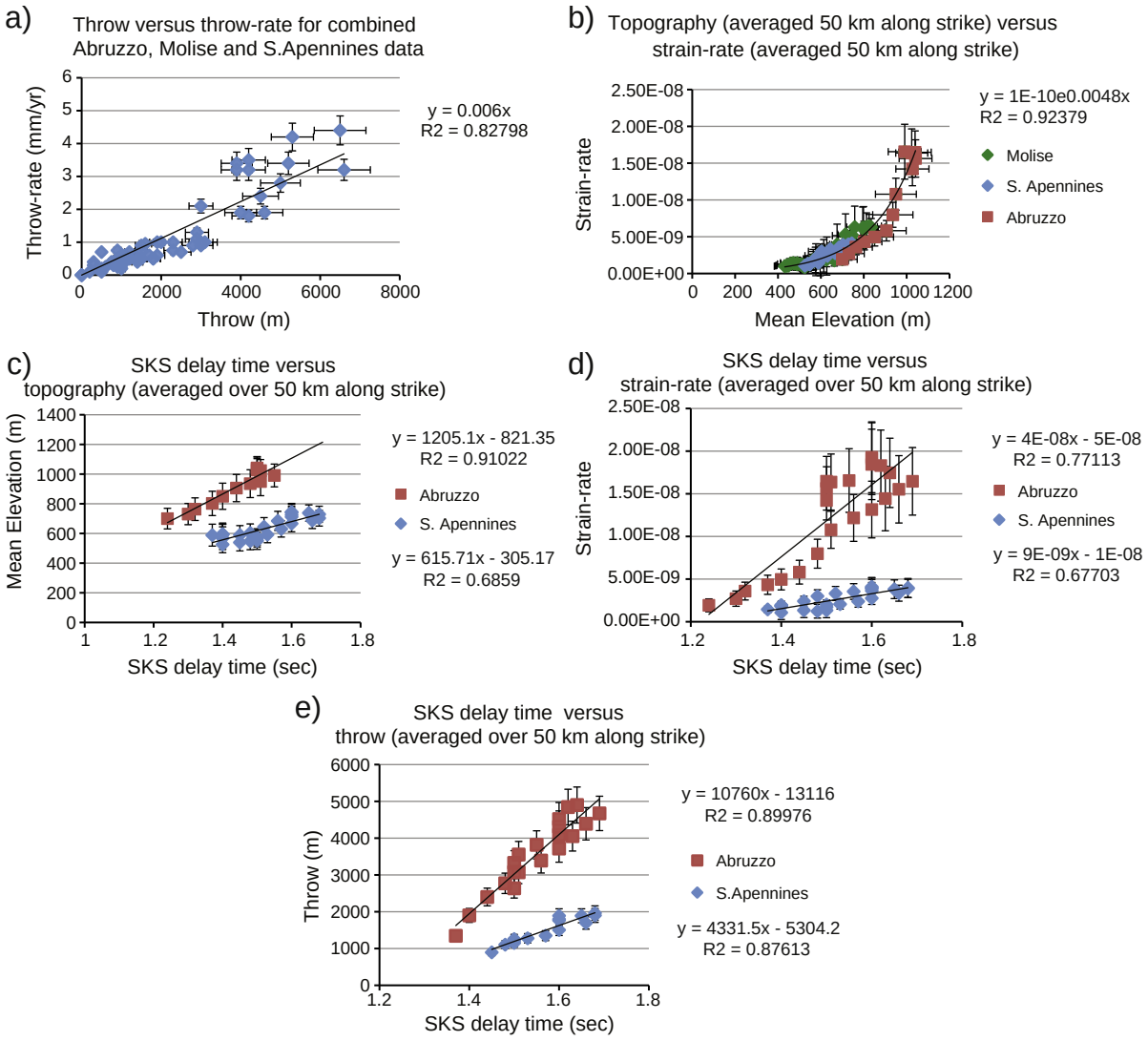

Fig. 4. Correlations between strain-rate, mean elevation, cumulative strain in the upper crust, and SKS delay times in the mantle. Data from the area of the Fucino Lake Bed have been excluded because very high values for slip-rate on local faults are defeating the regional uplift and incision to produce an interior drainage basin. This anthropogenically-drained lake is found within the largest example of a hydrologically closed basin in the Apennines, that has formed due to relatively-high values for local normal fault throw rates (1–2 mm/yr; these values approach or exceed uplift rates measured geodetically — see D'Anastasio et al. (2006); 1.0–1.5 mm/yr). Thus, although this local patch of high fault slip-rates has produced some of the highest values for relief across active normal faults in the central and southern Apennines (1729 m relief across the Velino fault between Magliano at 716 m [hangingwall] and Monte Velino at 2445 m [footwall]), and deeply-incised footwall drainage (Gole di Celano with c. 1000 m of incision), this obscures the regional strain-rate/elevation signal, hence why we have excluded the data. Errors in (a) and (e) from Roberts and Michetti (2004) and Papanikolaou and Roberts (2007). Errors in (b), (c) and (d) from Supplementary Table 3 (see Method section for more detail on errors).

and Roberts, 2007; Roberts and Michetti, 2004). These cross-sections demonstrate offsets of up to 2 km on individual faults that have accumulated during the Quaternary and perhaps since 2–3 Ma. When summed across strike, these throw measurements record the spatial variation in finite strain produced during the extension (Fig. 3c and d).

It has long been known that destructive earthquakes in central and southern Italy occur along active normal faults located on the crest of the Apennines. It has been noted that (1) the active extension is concentrated along the main topographic ridge of the Apennines and (2) an increase in width of the zone containing active normal faults (between northings 4,800,000 and 4,600,000) correlates with the higher elevation and increased width of the topographic belt (D'Agostino et al., 2001). However, although it is known that extension is concentrated on the crest of the Apennines, and it is thought that the high topography appears to result from mantle upwelling suggesting a causal link between mantle processes and the extension (D'Agostino et al., 2001), to date we are unaware of any study that demonstrates a correlation between the mean elevations and strain-rates in the upper crust. By searching for a correlation between mean elevation and strain-rates, we provide a test of the hypothesis that uplift driven by mantle upwelling causes the extension.

3. Method

In order to calculate strain-rates we modify equations presented by Kostrov (1974) that allow us to convert field measurements of the directions and amounts of slip on active normal faults since 15 ± 3 ka into strain-rates within boxes whose map dimensions we can define. In this case we define 5×5 km boxes (see Faure Walker (2010), Faure Walker et al. (2010), that we combine into 5×90 km boxes that traverse the Apennines in a NE–SW direction, parallel to the extension direction and minimum stress orientation (Roberts and Michetti, 2004). A full derivation of the equations involved is available (Faure Walker (2010); Faure Walker et al. (2010)), but we summarise the main relationships below.

Kostrov (1974) demonstrated that, if all the strain in a volume is seismic and the dimensions of the faults are small relative to the region, the average strain tensor, $\bar{\varepsilon}_{ij}$, within the volume can be obtained by summing the moment tensors of all the earthquakes occurring along faults within it:

$$\bar{\varepsilon}_{ij} = \frac{1}{2\mu V}\sum_{k=1}^{K} M_{ij}^{k} \quad (1)$$

where $\bar{\varepsilon}_{ij}$ represents the ith component of strain acting on the plane normal to the jth axis, M_{ij}^{k} is the ijth component of the moment tensor of the kth earthquake occurring within a volume V, and μ is the shear modulus. K is the total number of earthquakes in the volume V. However, following Molnar, and England and Molnar (England and Molnar, 1997; Molnar, 1983), here we modify this relationship to consider kinematic and deformation rate data for active faults since 15 ± 3 ka instead of individual earthquakes. We make use of the following field measurements: fault strike (Φ), dip (ϑ), slip direction (φ), plunge (p), throw (T) and length of the fault (L).

Expressing Eq. (1) in terms of independent components that can be measured in the field and including terms that define a time period over which we measure deformation rates gives the following equations for the horizontal principal strain-rate axis angle (θ) and the strain rate in this direction ($\dot{\bar{\varepsilon}}_{1'1'}$) and perpendicular to it ($\dot{\bar{\varepsilon}}_{2'2'}$):

$$\theta = \frac{1}{2}arctan\left(\frac{\sum_{k=1}^{K} L^k T^k cot\, p^k cos\left(\varphi^k + \Phi^k\right)}{\sum_{k=1}^{K} L^k T^k cotp^k sin\left(\varphi^k + \Phi^k\right)}\right) \quad (2)$$

$$\dot{\bar{\varepsilon}}_{1'1'} = \frac{1}{2at}\sum_{k=1}^{K}\left\{L^k T^k cot\, p^k\left[sin\left(\varphi^k - \Phi^k\right) + sin\left(\varphi^k + \Phi^k + arctan\left(\frac{\sum_{k=1}^{K} L^k T^k cotp^k cos\left(\varphi^k + \Phi^k\right)}{\sum_{k=1}^{K} L^k T^k cotp^k sin\left(\varphi^k + \Phi^k\right)}\right)\right)\right]\right\} \quad (3)$$

$$\dot{\bar{\varepsilon}}_{2'2'} = \frac{1}{2at}\sum_{k=1}^{K}\left\{L^k T^k cot\, p^k\left[sin\left(\varphi^k - \Phi^k\right) - sin\left(\varphi^k + \Phi^k + arctan\left(\frac{\sum_{k=1}^{K} L^k T^k cotp^k cos\left(\varphi^k + \Phi^k\right)}{\sum_{k=1}^{K} L^k T^k cotp^k sin\left(\varphi^k + \Phi^k\right)}\right)\right)\right]\right\}. \quad (4)$$

We use these equations to calculate the components of the average strain-rate tensor in the horizontal principal directions within 5×90 km boxes on a Universal Transverse Mercator (UTM) map projection within the Italian Apennines (Fig. 1). The data defining the amounts and directions of slip across active faults used in this study come from new fieldwork (Supplementary Table 1) that augments data presented in the literature (Boncio et al., 2004; Cinque et al., 2000; Di Bucci et al., 2002; Faure Walker, 2010; Faure Walker et al., 2010; 2009, Michetti et al., 1996, Papanikolaou and Roberts, 2007; Papanikolaou et al., 2005, Pizzi and Pugliese, 2004; Roberts, 2008; Roberts and Michetti, 2004; Salvi et al., 2003) (Supplementary Table 2) (e.g. See Fig. 3a, b and e). The data document spatial variation in throws across active normal faults that have accumulated since 15 ± 3 ka recorded at 123 sites along the major normal faults using chain surveying techniques, handheld laser range finders, total stations and LiDAR laser scans, and 13,280 measurements of the slip-direction that include the strike, dip, slip-direction, and plunge of the slip-direction at 222 sites made using compass and clinometer measurements of striated and corrugated fault planes. Comparison of our fault map with active fault maps from other research groups (Galadini and Galli, 2000; ISPRA, 2007; Pace et al., 2006; Schlagenhauf, 2009) is favourable, suggesting that there is broad agreement on the locations of active faults, and that we have not omitted major faults mentioned elsewhere in the literature.

Topographic profiles located along the centre of the 5×90 km boxes were constructed from SRTM 90 m DEM data using GeoMapApp. Each of the topographic data sets are orientated southwest–northeast and separated along-strike by 5 km intervals. Spot heights along the topographic profiles were sampled approximately every 850 m and used to sample the mean elevation for each profile and study the long wavelength topography. The 5 km width transects were also combined to calculate the mean elevation within 20×90 km transects (Fig. 3g and Supplementary Figure A1). The 95% confidence intervals of the mean elevation were calculated for each topographic profile using the assumption of a normal distribution in the topograpic spot heights:

Given a sample size n from a normal population with variance σ^2, a 95% confidence interval for the population mean is given by:

$$\left[\bar{x} - 1.96\frac{\sigma}{\sqrt{n}}, \bar{x} + 1.96\frac{\sigma}{\sqrt{n}}\right] \quad (5)$$

where $\bar{x}$ is the sample mean.

The mean elevations for each profile were then plotted to show how the topography changes along the length of the Apennines (Fig. 2).

In order to produce cross-plots that investigate the relationships between strain-rate and topography presented herein, and cumulative throw and SKS delay times from the literature (Fig. 4), values were projected across strike onto a transect running through the centres of the strain-rate bars in Fig. 1b. SKS delay times from Lucente and Margheriti (2008) were sampled along the same transect. Errors in strain-rate incorporate both the uncertainty in the age of the offset landforms (15 ± 3 ka), and variability in measured offset (± 1 m), and errors were summed where values for individual faults were summed across strike (Figs. 1, 2, 3a and 4). Variability of 1 m in vertical offset across an individual scarp over distances of a few tens of metres is typical, quantified by variability measured with millimetre precision from thousands of scarp profiles measured with ground-based LiDAR. Errors in cumulative throw are set by the thicknesses of Mesozoic and Cenozoic formations offset across the active faults recorded on published geological maps, because the formation thicknesses control the resolution of throw measurements. Throw errors for individual locations on faults are on the order of ± 100 m (Papanikolaou and Roberts, 2007; Roberts and Michetti, 2004), and errors have been summed where values from individual faults were summed across strike.

4. Results: relationships between faulting and topography

The principal horizontal strain-rates averaged since 15 ± 3 ka in $90\ km \times 5$ km transects across the Apennines are shown in Figs. 1 and 2 (strain-rates perpendicular to these values are stated in Supplementary Table 3). The extensional strain-rates are greatest in the northwest of the study area (Abruzzo-Lazio), they are low in the central section (Molise and NW Campania) and then appear to increase slightly in the southeast of the study area (SE Campania and Basilicata). The greatest strain-rate associated with a 5×90 km transect is found crossing the Fucino basin, Abruzzo, ($3.41^{+0.83}_{-0.40} \times 10^{-8}$ /yr) corresponding to an extension-rate of $3.1^{+0.7}_{-0.4}$ mm/yr (Fig. 2). Within the southern Apennines, the greatest strain-rate associated with a 90 km transect is $6.71 \pm 2.26 \times 10^{-9}$/yr, corresponding to an extension-rate of 0.6 ± 0.2 mm/yr. Extension does continue NW and S of our study area into Umbria and Calabria respectively, but we are unaware of published 15 ± 3 ka throw-rate and 2–3 Ma throw data summed across strike so it is not yet possible to compare our data with these regions. However, for the area we study, in order to investigate whether the aforementioned geographic pattern of strain-rates only applies since 15 ± 3 ka, or conversely, is consistent with strain accumulation over a longer period of the history of faulting,

we have plotted values of throw-rate summed across strike against values of cumulative throw summed in the same way (Figs. 3a–d and 4a). As mentioned above the cumulative throws have developed during the Quaternary and perhaps since 2–3 Ma (Roberts and Michetti, 2004). We find a strong relationship between throw measured over 2–3 Myrs along each transect and throw-rate measured in the same way ($R^2 = 0.828$; Fig. 4a). We interpret this to mean that the post 15 ± 3 ka strain-rate field is a long-lived feature of the deformation of the Apennines as it has dominated the throw accumulation on faults that have been active during the Quaternary and perhaps since 2–3 Ma (Roberts and Michetti, 2004).

Fig. 2 shows the relationships between strain-rates averaged since 15 ± 3 ka and the mean elevation within 5×90 km box transects. High extensional strain rates across the central and southern Apennines (0.4–3.0 mm/yr) are found in 5×90 km boxes with mean elevation of >600 m; boxes with <600 m mean elevation have extension rates <0.4 mm/yr. Strain-rates and the mean elevations calculated in 20×90 km transects show the same shape and trends, but with a smoothed signal (Fig. 3g, Supplementary Figure A1 and Supplementary Table 4). Note that values of topographic gradient averaged along NE–SW transects across the width of the Italian peninsula would show a similar spatial pattern. This is because the Apennines are sub-parallel to 2 coastlines at sea-level, and both coastal plains are approximately equidistant from the transect line we have chosen running through the strain-rate bars in Fig. 1b (see England and Molnar (2005) for the significance of topographic gradients in continental deformation). The areas of high post 15 ± 3 ka strain-rate and relatively-high elevation/gradient coincide with areas with high values for throw summed across strike (Fig. 3a–d). We interpret this to mean that the relationship between strain-rate and elevation/slope is long-lived, as a strain-rate field similar to that measured post 15 ± 3 ka has dominated throw accumulation in the Quaternary and perhaps since 2–3 Ma (Fig. 4a). This also suggests that fault lengths were established early in the deformation.

To investigate the strength of the relationship between 15 ± 3 ka strain-rate and mean elevation, we have plotted values of mean elevation in each 90 km × 5 km box, averaged over 50 km along strike, against strain-rate averaged in the same way; we find a strong correlation ($R^2 = 0.924$; Fig. 4b). We choose the 50 km length scale as it is longer than the length of individual faults (20–30 km), thus averaging out short length scale variations due to displacement gradients on faults and pre-faulting topography due to local erosion. Note that the relationship appears to be non-linear, and we discuss this below.

Overall, for the central and southern Apennines, there are clear correlations between the spatial variation in upper crustal strain-rates, finite strain in the upper crust, and mean elevation.

5. Discussion

We have demonstrated for the first time quantitative correlations between elevation, upper-crustal strain-rate and upper-crustal finite strain within the central and southern Apennines. If the topography is controlled by active uplift that has been in operation during the Quaternary, and uplift results from the mantle upwelling envisaged by D'Agostino et al. (2001), the correlation between elevation/slope, upper crustal strain-rate and finite strain is consistent with the hypothesis that "mantle upwelling beneath the central Apennines has been the dominant geodynamical process during the Quaternary, controlling both the geomorphological evolution and the distribution of active deformation" (D'Agostino et al., 2001).

Furthermore we point out that strain-rates, finite strains and elevation measured in the upper crust correlate with measurements that include the influence of the mantle (Figs. 3h–i and 4c–e). Firstly, free air gravity values are high (140–160 mGals; Fig. 3h) in the along strike position where upper crustal extension rate and finite throw values are high (0.4–3.1 mm/yr; 2–7 km cumulative throw summed across strike; Fig. 3a–d), and low (120 mGals) where upper crustal extension rate and finite throw values are low (<0.4 mm/yr; <2 km cumulative throw). Secondly, SKS splitting delay times vary along the strike of the Apennines (Fig. 3h). Lucente and Margheriti (2008) interpolated individual splitting time delays over a 10° latitude and 10° longitude grid. Two maxima in these interpolated delay times in the Apennines (c. 1.3–1.7 s) coincide spatially with the two areas that exhibit peaks in post 15 ± 3 ka strain-rate, finite strain, mean elevation and free air gravity; the area between these peaks is characterised by a shorter SKS delay time of 0.8–1.3 s (see Lucente and Margheriti (2008), their Fig. 1, and our Fig. 3h). In order to quantify these correlations, Fig. 4 shows that (1) SKS delay times in the mantle correlate with mean elevation in 90 km × 5 km transects (Fig. 4c; $R^2 = 0.910$ and 0.686), (2) SKS delay times in the mantle correlate with upper crustal post 15 ± 3 ka strain-rates (Fig. 4d; $R^2 = 0.771$ and 0.677), and (3) SKS delay times in the mantle correlate with throws across faults in the upper crust that have developed during the Quaternary and perhaps since 2–3 Ma (Fig. 4e; $R^2 = 0.899$ and 0.876). We discuss the differences in these correlations for Abruzzo and the S. Apennines below. However, before this, we note that SKS anisotropy is thought to record alignment of olivine crystals in the mantle and hence cumulative strain in the mantle; longer SKS delay times indicate stronger anisotropy and hence higher strains in the mantle. Thus, we suggest that two peaks in upper crustal strain-rate, finite strain and mean elevation overlie two peaks in strain in the mantle evidenced by SKS delay times. These correlations (Fig. 4), together with evidence of dynamic support of the topography in the Apennines (D'Agostino et al., 2001), suggest that mantle flow influences rates and amounts of extension in the upper crust. We suggest that this coupling between mantle flow and upper-crustal extension is long-lived, evidenced by the fact that cumulative throws across faults that have developed over the Quaternary and perhaps since 2–3 Ma, when summed across strike, correlate with summed offsets that have accumulated since 15 ± 3 ka, and so in turn correlate with mean elevation, Free Air Gravity data and SKS delay times (Fig. 3c and d). These correlations are consistent with the hypothesis that mantle flow influences rates of extension in the upper-crust, and also suggests that such coupling has influenced the throws and hence long-term growth rates of the faults during the Quaternary and perhaps since 2–3 Ma.

The different correlations that exist between SKS delay time and elevation, strain-rate and finite strain for the southern Apennines and Abruzzo in the central Apennines (Fig. 4c–e) suggest that coupling between mantle strain accumulation and upper crustal strain accumulation differs between these two regions. We note the difference in upper crustal strain-rate over 15 ± 3 ka for these two regions. It may be that there is a non-linear rheological relationship between the driving force and strain-rate, explaining the non-linear relationship between mean elevation and strain-rate shown in Fig. 4b; however, it is clear that this needs to be studied further, with rheological modelling, before firm conclusions can be drawn.

We speculate that the reason why mantle flow influences upper-crustal extension may be that the north and south edges of the Central Apennines Slab Window imaged using P-wave tomography (Rosenbaum et al., 2008; Wortel and Spakman, 2000, Fig. 3i), coincide geographically, when projected onto our transect line, with the two peaks in upper crustal strain-rate and strain overlying two peaks in strain in the mantle (Figs. 3, 4 and 5). Asthenospheric mantle may be being forced through the window in the sinking slab, as suggested by Lucente et al. (2006) (see their Fig. 5d), producing higher strain-rates in the mantle close to the edges of the slab window due to bunching of the stream lines. Slab pull forces may also be concentrated at the edges of the torn slab (Wortel and Spakman, 2000). Moreover, experimental studies of mantle flow associated with broken subducting slabs predict a component of upward force associated with toroidal flow around slab edges from the high-pressure bottom

side of the slab to the low-pressure top side (Piramallo et al., 2006; Schellart, 2004; Stegman et al., 2006; Zattin et al., 2000). This upward force may provide a plausible mechanism to explain the uplift and high topography, although the magnitude of the uplift that could be produced in this way is unconstrained by our study. This physical mechanism for uplift is consistent with the ideas of D'Agostino et al. (2001) in that topography is supported dynamically by motion of the mantle. However, in the scenario suggested herein, the motions and strain-rates would be controlled predominantly by pressure gradients produced by mantle flow and constriction to this flow represented by the slab window, rather than solely by temperature gradients. This hypothesis implies that the age of the slab window is Quaternary and perhaps as old as 2–3 Ma (see Roberts and Michetti (2004) for a summary of the debate concerning the age of the initiation of extension). We note that Rosenbaum et al. (2008), using magmatic evidence, have suggested that tears in the slab were developing as far back as at least 4–6 Ma, with slab break and slab window formation at ~2 Ma.

If we are correct that mantle flow controls strain-rates in the upper crust in the Apennines, it follows that mantle flow will control the geography of seismic hazard in the region, as seismic hazard is controlled by rates of slip across active normal faults. As fault specific earthquake recurrence intervals for a given magnitude are inversely proportional to the slip-rates on faults, one would expect more earthquakes of a given magnitude per unit time in regions with higher upper crustal strain rates. Thus, one would expect the number of earthquakes per unit time of a given magnitude to vary along the strike of the Apennines. However, we are left with a problem because it is well-known that horizontal principal strain-rates derived from summation of moment tensors for large (>Mw 6) historical earthquakes since 1349 A.D. (Selvaggi, 1998), and shear strain rates from GPS re-occupation of a 1875 A.D. triangulation network (Hunstad et al., 2003) show little if any significant difference in strain-rate along the strike of the Apennines (although, GPS rates from Serpelloni et al. (2005) are higher in the central Apennines, by a factor of about 2, than in Molise-north Campania and the southern Apennines). The problem is how to reconcile the strain-rate field since 15 ± 3 ka, that correlates with mantle strains and finite upper crustal strains, perhaps over 2–3 Myrs, with the differing strain-rate fields implied by <c. 100 year-averaged geodetic and moment summation data. We suggest the following way to reconcile strain-rate fields over different timescales: (1) spatial strain-rate variations measured over numerous seismic cycles (15 ± 3 kys) and longer (2–3 Myrs) that correlate with mean elevation, free-air gravity and SKS splitting delay times should be considered to be the 1st order measure of the geography of seismic hazard; (2) deviations from the 1st order measure, derived over timescales that are short (<c. 100 yrs) relative to the seismic cycle (hundreds to thousands of years) (e.g. historical seismicity and geodesy) provide important data on the natural temporal variability in the strain-rate field; (3) study of deviations from the 1st order measure could be inverted to derive the efficacy of second order controls on earthquake recurrence such as triggering via Coulomb stress transfer (Cowie and Roberts, 2001) or fluid effects (Miller et al., 2004; Terakawa et al., 2010) that may operate on shorter timescales and lengthscales.

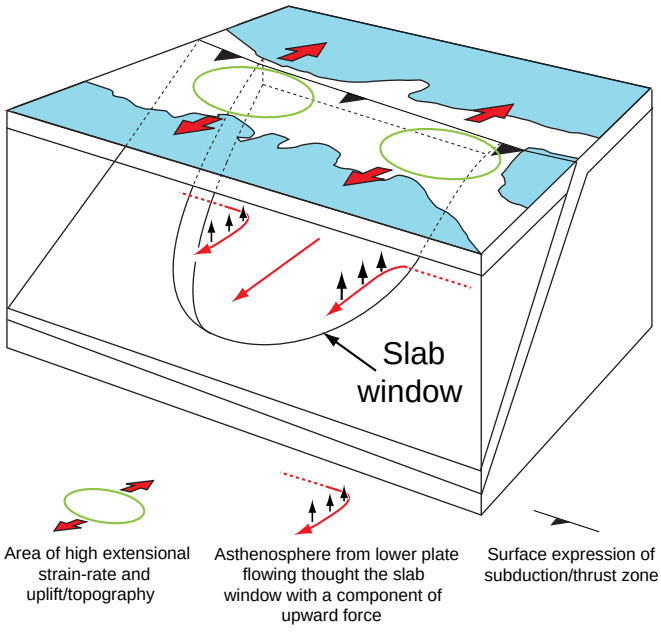

Fig. 5. 3D cartoon of the geometry of extension and uplift in the Apennines relative to the geometry of the central Apennines Slab Window (modified from Lucente et al. (2006)), and asthenospheric flow through the slab window (modified from Lucente et al. (2006)).

6. Conclusions

Active normal faults in Italy are localised on the crest of a ~200 km topographic bulge elongated along the strike of the Apennines. Spatial variations in upper crustal strain-rate and finite strain across these faults correlate with spatial variations in mean elevation, free-air gravity and SKS splitting delay times for the Italian Apennines. High extension rates across these faults (0.4–3.1 mm/yr in 5×90 km boxes traversing the Apennines) are associated with finite cumulative throws of 2–7 km, mean elevation of >600 m, free-air gravity values of 140–160 mGals, and SKS delay times of 1.2–1.8 s; boxes with <600 m mean elevation have extension rates<0.4 mm/yr, cumulative finite throws of <2 km, free-air gravity values of 120 mGals, and SKS delay times of 0.8–1.2 s. The strong relationships between these variables ($R2 = 0.92$–0.67; see Fig. 4) suggest that flow in the mantle, perhaps controlled by flow through the slab window, produces uplift that drives active extension in the upper crust and thus controls seismic hazard in the region.

Supplementary materials related to this article can be found online at doi:10.1016/j.epsl.2012.01.028.

Acknowledgements

This study was funded by a studentship to J.P. Faure Walker (NER/S/A/2006/14042) and NERC Grants NE/H003266/1, NE/E01545X/1, NE/B504165/1, GR9/02995 and NE/I024127/1.

References

Ambrosetti, P., Carraro, F., Deiana, G., Dramis, F., 1982. Il sollevamento dell'Italia Centrale tra il Pleistocene inferiore e il Pleistocene medio. C.N.R. P.F.G., 513, pp. 219–223.
Anderson, H., Jackson, J., 1987. Active tectonics of the Adriatic region. Geophys. J. Int. 91 (3), 937–983.
Anzidei, M., Boschi, E., Cannelli, V., Devoti, R., Esposito, A., Galvani, A., Melini, D., Pietrantonio, G., Riguzzi, F., Sepe, V., Serpelloni, E., 2009. Coseismic deformation of the destructive April 6, 2009 L'Aquila earthquake (central Italy) from GPS data. Geophys. Res. Lett. 36. doi:10.1029/2009GL039145.
Atzori, S., Hunstad, I., Chini, M., Salvi, S., Tolomei, C., Bartolini, C., Caputo, R., Pieri, M., 1996. Pliocene-Quaternary sedimentation in the northern Apennine foredeep and related denudation. Geol. Mag. 133 (3), 255–273.
Beccaluva, L., Brotzu, P., Macciotta, G., Morbidelli, L., Serri, G., Traversa, G., 1989. Cainozoic tectono-magmatic evolution and inferred mantle sources in the Sardo-Tyrrhenian area. In: Boriani, A., Bonafede, M., Piccardo, G.B., Vai, G.B. (Eds.), The lithosphere in Italy. Accademia dei Lincei, Rome, pp. 229–248.
Boncio, P., Lavecchia, G., Milana, G., Rozzi, B., 2004. Seismogenesis in central Apennines, Italy: an integrated analysis of minor earthquake sequences and structural data in the Amatrice-Campotosto area. Ann. Geophysics 47 (6), 1723–1740.
Bordoni, P., Valensise, G., 1998. Deforemation of the 125ka marine terrace in Italy: tectonic implications. In: Stewart, I., Vita-Finzi, C. (Eds.), Coastal Tectonics, Vol. 146, pp. 71–110.
Cantalamessa, G., Centamore, E., Chiocchini, U., Colalongo, M.L., Micarelli, A., Nanni, T., Pasini, G., Potetti, M., Lucchi, F.R., 1986. Il Plio-Pleistocene delle Marche.

Cavinato, G.P., De Celles, P.G., 1999. Extensional basins in the tectonically bimodal central Apennines fold-thrust belt, Italy: response to corner flow above a subducting slab in retrograde motion. Geology 27 (10), 955–958.
Cinque, A., Ascione, A., Caiazzo, 2000. Distribuzione spazio-temporale e caratterizzazione della fagliazione quaternaria in Appennino meridionaleDistribuzione spazio-temporale e caratterizzazione della fagliazione quaternaria in Appennino meridionale. CNR-Gruppo Nazionale per la Difesa dai Terremoti - Roma, pp. 203–218.
Cowie, P.A., Roberts, G.P., 2001. Constraining slip rates and spacings for active normal faults. J. Struct. Geol. 23, 1901–1915.
D'Agostino, N., Jackson, J., Dramis, F., Funiciello, R., 2001. Interactions between mantle upwelling, drainage evolution and active normal faulting: an example from the central Apennines (Italy). Geophys. J. Int. 147, 475–497.
D'Agostino, N., Avallone, A., Cheloni, D., D'Anastasio, E., Mantenuto, S., Selvaggi, G., 2008. Active tectonics of the Adriatic region from GPS and earthquake slip vectors. J. Geophys. Res. 113, B12413.
D'Anastasio, E., De Martini, P.M., Selvaggi, G., Pantosti, D., Marchioni, A., Maseroli, R., 2006. Short-term vertical velocity field in the Apennines (Italy) revealed by geodetic levelling data. Tectonophysics 418, 219–234.
Demangeot, J., 1965. Geomorphologie des Abruzzes Adriatiques. No. 403. Mem. Documents, Centre Rech. Docum. Cartogr., num. H.s. CNRS, Paris, p. 403.
Di Bucci, D., Corrado, S., Naso, G., 2002. Active faults at the boundary between central and southern Apennines (Isernia, Italy). Tectonophysics 359, 47–63.
Doglioni, C., 1995. Geological remarks on the relationship between extension and convergent geodynamic settings. Tectonophysics 252, 253–267.
Dramis, F., 1992. Il ruolo dei sollevamenti tettonici a largo raggio nella genesi del rilievo appenninico. Studi Geologici Camerti, Vol. Spec. 1992/1, pp. 9–15.
Dufaure, J.J., Bossuyt, D., Rasse, M., 1989. Deformations quaternaires et morphogenese de l'Apennin Central adriatique. Physio-Géo 18, 9–46.
England, P., Molnar, P., 1997. Active deformation of Asia: from kinematics to dynamics. Science 278, 647–650.
England, P., Molnar, P., 2005. Late Quaternary to decadal velocity fields in Asia. J. Geophys. Res. 110 (B12401). doi:10.1029/2004JB003541.
Faure Walker, J. P., 2010. Mechanics of continental extension from Quaternary strain field in the Italian Apennines. Ph.D. thesis, University College London.
Faure Walker, J.P., Roberts, G.P., Cowie, P.A., Papanikolaou, I., Michetti, A.M., Sammonds, P., Phillips, R., 2009. Horizontal strain-rates and throw-rates across breached relay-zones, central Italy: implications for the preservation of throw deficits at points of normal fault linkage. J. Struct. Geol. 31. doi:10.1016/j.jsg.2009.06.01), 1145-1160.
Faure Walker, J.P., Roberts, G.P., Sammonds, P., Cowie, P.A.C., 2010. Comparison of earthquake strains over 100 and 10,000 year timescales: insights into variability in the seismic cycle in the central Apennines, Italy. J. Geophys. Res. 115 (B10418). doi:10.1029/2009JB006462.
Ferranti, L., Oldow, J.S., 2005. Latest Miocene to Quaternary horizontal and vertical displacement rates during simultaneous contraction and extension in the Southern Apennines orogen, Italy. Terra Nova 17, 209–214.
Galadini, F., Galli, P., 2000. Active tectonics in the Central Apennines (Italy) — input data for seismic hazard assessment. Nat. Hazard. 22, 225–270.
Galadini, F., Messina, P., Giaccio, B., Sposato, A., 2003. Early uplift history of the Abruzzi Apennines (central Italy): available geomorphological constraints. Quat. Int. 101–102, 125–135.
Ghisetti, F., Vezzani, L., 1999. Depth and modes of Pliocene–Pleistocene crustal extension of the Apennines (Italy). Terra Nova 11, 67–72.
Gliozzi, E., Mazzini, I., 1998. Paleoenvironmental analysis of Early Pleistocene brackish marshes in the Rieti and Tiberino intraappenninic basins (Latium and Umbria, Italy) using ostracods (Crustacea). Palaeogeogr. Palaeoclimatol. Palaeoecol. 140, 325–333.
Hooker, P.J., Bertrami, R., Lombardi, S., O'Nions, R.K., Oxburgh, E.R., 1985. Helium-3 anomalies and crust-mantle interactions in Italy. Geochim. Cosmochim. Acta 49, 2505–2513.
Hunstad, I., Selvaggi, G., D'Agostino, N., England, P., Calrke, P., Pierozzi, M., 2003. Geodetic strain in peninsular Italy between 1875 and 2001. Geophys. Res. Lett. 30 (4), 1181–1184.
ISPRA, 2007. Ithaca projectURL http://www.apat.gov.it/site/en-GB/Projects2007.
Italiano, F., Martelli, M., Martinelli, G., Nuccio, P.M., 2000. Geochemical evidence of melt intrusions along lithospheric faults of the Southern Apennines, Italy: geodynamic and seismogenic implications. J. Geophys. Res. 105, 13569–13578.
Jolivet, L., Facenna, C., Goffe, B., Mattei, M., Rosseti, F., Brunet, C., Storti, F., Funiciello, R., Cadet, J.P., D'Agostino, N., Parra, T., 1998. Midcrustal shear zones in postorogenic extension: example from the northern Tyrrhenian Sea. J. Geophys. Res. 103 (B6), 12123–12160.
Kostrov, V.V., 1974. Seismic moment and energy of earthquakes, and seismic flow of rock. Izv. Earth Phys. 1, 23–40 (translation UDC 550.341, pp13–21)..
Lucente, F.P., Margheriti, L., 2008. Subduction rollback, slab breakoff, and induced strain in the uppermost mantle beneath Italy. Geology 36 (5), 375–378.
Lucente, F.P., Margheriti, L., Piromallo, C., Barruol, G., 2006. Seismic anisotropy reveals the long route of the slab through the western-central Mediterranean mantle. Earth Planet. Sci. Lett. 241, 517–529.
Mancini, M., D'Anastasio, E., Barbieri, M., Martini, P.M.D., 2007. Geomprphological, paleontological and 87sr/86sr isotope analyses of early Pleistocene paleoshorelines to define the uplift of Central Apennines (Italy). Quat. Res. 67, 487–501.
Marinelli, G., Barberi, F., Cioni, R., 1993. Sollevamenti neogenici e intrusioni acide della Toscana e del Lazio settentrionale. Mem. Soc Geol. Ital. 49, 279–288.
Mazzanti, R., Trevisan, L., 1978. Evoluzione della rete idrografica nell'Appennino centro-settentrionale. Geogr. Fis. Dinam. Quat. 1, 55–62.
Mazzoli, S., Helman, M., 1994. Neogene patterns of relative plate motions for Africa-Europe: some implications for recent central Mediterranean tectonics. Geol. Rundsch. 83, 464–468.
Mele, G., Rovelli, A., Seber, D., Barazangi, M., 1996. Lateral variations of Pn propagation in Italy: evidence for a high-attenuation zone beneath the Apennines. Geophys. Res. Lett. 23, 709–712.
Mele, G., Rovelli, A., Seber, D., Barazangi, M., 1997. Shear wave attenuation in the lithosphere beneath Italy and surrounding regions; tectonic implications. J. Geophys. Res. 102, 11863–11875.
Mele, G., Sandvol, E., Cavinato, G.P., 2006. Evidence of crustal thickening beneath the central Apennines (Italy) from teleseismic receiver functions. Earth Planet. Sci. Lett. 249, 415. doi:10.1016/j.epsl.2006.05.024.
Michetti, A.M., Brunamonte, F., Serva, L., Vittori, E., 1996. Trench investigations of the 1915 Fucino earthquake fault scarps (Abruzzo, Central Italy): geological evidence of large historical events. J. Geophys. Res. 101 (B3), 5921–5936.
Miller, S.A., Colletini, C., Chiaraluce, L., Cocco, M., Varchiand, M., Kaus, B.J.P., 2004. Aftershocks driven by a high-pressure CO2 source at depth. Nature 427, 724–727.
Molnar, P., 1983. Average regional strain due to slip on numerous faults of different orientations. J. Geophys. Res. 88, 6430–6432.
Morewood, N., Roberts, G.P., 2000. The geometry, kinematics and rates of deformation within an en echelon normal fault boundary, central Italy. J. Struct. Geol. 22, 1027–1047.
Ori, G.C., Serafini, G., Visentini, G., Lucchi, F.R., Casnedi, R., Colalongo, M.L., Mosna, S., 1993. Depositional history of the Pliocene-Pleistocene Adriatic foredeep (Central Italy) from surface and subsurface data. In: Specer, A. (Ed.), Generation, accumulation and production of Europe's hydrocarbon III. Vol. 3. Special Publication. European Association of Petroleum Geoscientists, pp. 233–258.
Pace, B., Peruzza, L., Lavecchia, G., Boncio, P., 2006. Global seismogenic source modelling and probabilistic seismic hazard analysis in Central Italy. Bull. Seismol. Soc. Am. 96 (1), 107–132.
Papanikolaou, I.D., Roberts, G.P., 2007. Geometry, kinematics and deformation rates along the active normal fault system in the southern Apennines: implications for fault growth. J. Struct. Geol. 29, 166–188.
Papanikolaou, I.D., Roberts, G.P., Michetti, A.M., 2005. Fault scarps and deformation rates in Lazio-Abruzzo, Central Italy: comparison between geological fault slip-rate and GPS data. Tectonophysics 408, 147–176.
Piramallo, C., Becker, T.W., Funiciello, F., Facenna, C., 2006. Three-dimensional instantaneous mantle flow induced by subduction. Geophys. Res. Lett. 33 (L08304). doi:10.1029/2005GL025390.
Pizzi, A., Pugliese, G., 2004. InSAR-DEM analyses integrated with geologic field methods for the study of long-term seismogenic fault behavior: Applications in the axial zone of the central Apennines (Italy). J. Seismol. 8, 313–329.
Pizzi, A., Calamita, F., Coltori, M., Pieruccini, P., 2002. Quaternary normal faults, intramontane basins and seismicity in the Umbria-Marche Apennines Ridge (Italy): contribution of neotectonic analysis to seismic hazard assessment. Boll. Soc. Geol. It. speciale. (1), 923–929.
Roberts, G.P., 2008. Visualisation of active normal fault scarps in the Apennines, Italy: a key to assessment of tectonic strain release and earthquake rupture.
Roberts, G.P., Michetti, A.M., 2004. Spatial and temporal variations in growth rates along active normal fault systems: an example from the Lazio-Abruzzo Apennines, central Italy. J. Struct. Geol. 26, 339–376.
Rosenbaum, G., Gasparon, M., Lucente, F.P., Peccerillo, A., Miller, M., 2008. Kinematics of slab tear faults during subduction segmentation and implications for Italian magmatism. Tectonics 27. doi:10.1029/2007TC002143.
Salvi, S., Cinti, F.R., Collini, L., D'Addezio, G., Doumaz, F., Pettinelli, E., 2003. Investigation of the active Celano-L'Aquila Fault System, Abruzzi (central Apennines, Italy) with combined ground penetrating radar and palaeoseismic trenching. Geophys. J. Int. 155, 805–818.
Schellart, W.P., 2004. Kinematics of subduction and subduction-induced flow in the upper mantle. J. Geophys. Res. 109 (B07401). doi:10.1029/2004JB002970.
Schlagenhauf, A., 2009. Identification des forts seismes passes sur les failles normales actives de la region Lazio-Abruzzo (Italie centrale) par "datations cosmogeniques" (36Cl) de leurs escarpments. Ph.D. thesis, l'Universite Joseph Fourier,, Grenoble, France
Selvaggi, G., 1998. Spatial distribution of horizontal seismic strain in the Apennines from historical earthquakes. Ann. Geofis. 41 (2).
Serpelloni, E., Anzidei, M., Baldi, P., Casula, G., Galvani, A., 2005. Crustal velocity and strain-rate fields in Italy and surrounding regions: new results from the analysis of permanent and non-permanent GPS networks. Geophys. J. Int. 161, 861–880.
Serri, G., Innocenti, F., Manetti, P., 1993. Geochemical and petrological evidence of the subduction of delaminated Adriatic continental lithosphere in the genesis of the Neogene-Quaternary magmatism of central Italy. Tectonophysics 223, 117–147.
Stegman, D.R., Freeman, J., Schellart, W.P., Moresi, L., May, D., 2006. Influence of trench width on subduction hinge retreat rates in 3-D models of slab rollback. Geochem. Geophys. Geosyst. 7 (Q03012). doi:10.1029/2005GC001056.
Terakawa, T., Zoporowski, A., Galvan, B., Miller, S.A., 2010. High-pressure fluid at hypocentral depths in the L'Aquila region inferred from earthquake focl mechanisms. Geology 38, 995–998. doi:10.1130/G32457.1.
Walters, R.J., Elliott, J.R., D'Agostino, N., England, P.C., Hunstad, I., Jackson, J.A., Parsons, B., Phillips, R.J., Roberts, G.P., 2009. The 2009 L'Aquila earthquake (central Italy): a source mechanism and implications for seismic hazard. Geophys. Res. Lett. 36 (L17312). doi:10.1029/2009GL039337.
Wortel, M.J.R., Spakman, W., 2000. Subduction and slab detachment in the Mediterranean-Carpathian Region. Science 290, 1910–1917.
Zattin, M., Landuzzi, A., Picotti, V., Zuffa, G.C., 2000. Discriminating between tectonic and sedimentary burial foredeep succession, Northern Apennines. J. Geol. Soc. Lond. 157, 629–633.

Electronic Supplement

New throw-rate and slip direction data

Table 1: New data sites. Note only throws shown calculated from a scarp profile (column 6) or in square brackets (column 7) are used in calculation of strain-rates

fault	x utm	y utm	slip direction	slip plunge	15±3kyr throw measured from scarp profile (m)	notes on offsets of geomorphological features
Pozzilli	0421357	4597134	132	45	-	Smooth fault plane exposed by road with mm and 10cm scale oblique striations, exposed for approx. 20m along strike, cannot determine offset due to road - expect most of fault plane is exposed by excavation for road, could not see offset to SE away from road
Pozzilli	0421407	4597084	130	33	-	Limestone fault plane exposed by road, fault plane has very oblique striations, estimate approx 1m throw.
Pozzilli	0422255	4596601	225	71	-	Very degraded fault plane, some fracturing parallel to strike of fault, contact between scarp and lower slope is at a gradient, throw estimated between 0-5m, strike 190^o
Pozzilli	0427760	4592447	213	61	3.3	Scarp profile constructed using metre ruler [3.3m], poorly preserved fault plane near base of triangular facets.
Pozzilli	0430588	4590797	218	77	-	Limestone exposed almost continuously along strike (by road) for approx. 50m, clear mm scale striations on two approx 1sq.m planes, maximum height of exposure about 10m - throw difficult to determine due to road
Pozzilli	0432189	4589723	281	60	-	Fault plane exposed by road, cannot determine throw, unsure whether it is main fault plane or hangingwall fault, it is most likely within a few metres of the main fault plane
Boiano	0441865	4600008	101	41	-	-

Boiano	0442836	4599327	353	62	2.6	Scarp profile constructed using a metre ruler shows a [2.6m] offset (profile constructed across path), plane exposed by path and for approx. 8m along strike, steep upper and lower slope.
Boiano	0446590	4595063	029	82	-	-
Boiano	0456475	4592076	046	58	-	-
Boiano	0450693	4590651	019	70	-	Approx. NW striking planar limestone surface exposed by road, quite fractured behind, exposed semi-continuously along strike for approx. 8m and approx. 4m down dip, road next to plane prevents estimation of throw, no preferred orientation to fracturing on the plane, possibly some approx 8mm scale corrugations.
Boiano	0461244	4587763	352	68	-	-
Boiano	0461163	4587626	329	64	-	Fault plane exposed behind chicken wire next to road.
Boiano	0458615	4587389	012	46	6.6	Fault plane exposed in outside church, scarp profile constructed with metre ruler in woods, note this was done away from large fan surfaces, calculated throw [6.6m], but lower and upper slope are not parallel.
Irpinia	0516377	4519069	58	73	-	Very degraded semi-planar limestone surface which undulates with average strike approx. 330^o exposed by track for approx. 20m along strike and up to 6m down-dip. Slope appears to over-steepen, but track and shallower lower slope prevent estimations of offset. No free face.
Antithetic Irpinia	0543268	4514411	187	71	-	Limestone degraded scarp almost continuous along strike, estimate throw approx. 5m, small patches ($<$20cm) of smooth free face with striations.
Antithetic Irpinia	0543393	4514310			5.0	Profile constructed with metre ruler [5.0m] very degraded plane almost continuous along strike (120^o). No free face. Planar lower slope.

San Gregorio Magno	0533128	4502318			3.0	Degraded plane semi-continuous along strike for 10-20m at a time. Continuous grassy/prickly upper and lower slope, NB/ lower slope looks continuous all way down to valley but cannot continue profile due to impenetrable vegetation. Scarp profile constructed with a metre ruler [3.0m].
Alburni	0534691	4485310	329	28	-	Large planar limestone surface exposed for >20m along strike (approx. 320^o) and approx. 25m down-dip (not 15kyr offset), cut clasts present on planes, undefined Holocene/Pleistocene sediments seen outcropping on top of fault plane.
Val di Diano	0538184	4492468			8.4	Continuous scarp with planar limestone surface. Scarp profile constructed with metre ruler [8.4m].
Val di Diano	0538400	4492298	205	59	-	Continuous fault plane with large upper degraded slope, lower slope has many gullies.
Val di Diano	0538715	4491952	206	62	-	Plane within footwall of degraded scarp, polished in places, estimate throw between 7-9m (appears same as (fA1), crumbled limestone behind plane.
Val di Diano	0538756	4491945			10.1	Continuous scarp with planar limestone surface with fractured limestone behind, no free face, exposed for approx. 4m down-dip. Scarp profile constructed with metre ruler [10.1m].
Val di Diano	0545913	4479765			8.5	Very degraded scarp at top of cultivated slope, bottom of bedrock scarp possibly has free face exposed, strike approx. 140^o, along strike offset continues but limestone scarp does not, NB/ there are a few metres of bracken etc. between the scarp and the cultivated land, upper slope appears slightly steeper than lower slope, fractured limestone behind free face. Scarp profile constructed using metre rule [8.5m].
Val d'Agri	0575943	4465991	262	46	-	Limestone exposed by road, a few planes with striations

Maratea	0555869	4443186	226	52	-	Limestone fault plane exposed semi-continuously down-dip and along strike for 10s metres. Appears to have been excavated by abandoned quarry. Planar surface extends to under breccia/gravel. Some very smooth shiny surfaces. Planar surfaces preserved across undulations, axis of undulation has a trend 222^o.
Maratea	0562756	4428445	255	49	-	Very planar continuous limestone scarp undulating on a 2m scale with striations and cut clasts. Double line of cosmogenic sampling. Contact with lower slope is at an approx. 30^o angle as it is at the edge of a cone coming down from a gully from NE of site. Do not see any breccia cemented to fault plane.
Maratea	0562940	4428053	261	54	-	Continuous limestone scarp for hundreds of metres, degraded plane exposed for approx 14m down dip. Planes with striations on are 1.5-2m up from ground and have dimensions of order 1 sq.m.
Mercure	0582178	4429633			-	Scarp profile constructed using a metre ruler [6.6m], very degraded scarp with no free face, NB/ short lower slope as beyond profile the slope steepens into the path, then after the path there are a series of steps likely associated with tree roots.
Pollino	0590990	4416166	188	62	-	Fault plane preserved within scree/broken limestone by road, semi-continuous for approx 15m along strike, striations and cut clasts. Where fault plane is missing, the broken limestone behind is further eroded (i.e. fault plane acting as an erosion barrier). Broken segments of the plane (20-50cm diameter) are seen, which have fallen off. Strike/dip of outcrop approx. 120/60. NB/ Plane undulates on an approx 1.5-2m scale, note preserved planes are on one side of these undulations.

Piedmonte Matese	0446175	4578916	173	55	-	Triangular facets seen at top of fan, which pre-dates the Holocene (assumption from its great size), no offsets seen in fan from distance - max throw of 5m could be missed through trees, therefore assume throw is less than 5m
Letino	0436874	4588979	189	60	-	Fault plane exposed at side of road with matrix supported fault breccias on top of the plane and metre scale corrugations, striations seen in vadose calcite flow-stone suggesting it was sub aerial when grooves were formed, the road and cultivation of land prevents accurate estimation of throw, looking into distance estimate throw could be up to approx. 3m.
Miranda-Pesche	0438258	4609791	202	301	-	Limestone planes exposed for approx. 5m along strike and approx. 5m down dip by road, grooves on 0.5cm-10cm scale not pitted like water erosion, planes have approx. same dip as slope, 0.7-1.5m of soil on top of plane, note grooves are present under soil, large eroded boulders by road, in situ limestone breccia (on top) of where expect planes to meet in middle

Previously published throw-rate and slip direction data

Table 2: Previously published data collected using same method as this paper, note that locations from Morewood and Roberts [9] were assigned UTM coordinates in Faure Walker et al. [6]. For details of individual sites see relevent paper.

fault	x utm	y utm	slip direction	slip plunge	15 ± 3kyr throw (m)	source
Alburni	0521078	4490920	059	80	-	Papanikolaou and Roberts [11]
	0529594	4486994	034	48	-	Papanikolaou and Roberts [11]
	0535093	4484835	348	61	-	Papanikolaou and Roberts [11]
	0535103	4485272	358	44	-	Papanikolaou and Roberts [11]
	0536228	4484680	008	42	-	Papanikolaou and Roberts [11]
	0540187	4484648	342	46	-	Papanikolaou and Roberts [11]
Aquila	0391951	4679798	256	42	5	Roberts and Michetti [14]
	0391907	4679658	-	-	5.7	Papanikolaou et al. [12]
	0386594	4688439	-	-	3.5	Papanikolaou et al. [12]
	0385225	4687517	-	-	6.6	Papanikolaou et al. [12]
	0384225	4687552	-	-	3.5	Papanikolaou et al. [12]

	0383561	4689552	237	56	25	Roberts and Michetti [14]
	0383457	4689203	-	-	7	Papanikolaou et al. [12]
	0368500	4698400	198	38	-	Roberts and Michetti [14]
Aremogna-Cinque Miglia	0421485	4631217	221	57	11.6	Faure Walker et al. [6]
	0421801	4630850	216	35	7.1	Faure Walker et al. [6]
	0422111	4629669	244	57	-	Faure Walker et al. [6]
Assergi	0386260	4696767	214	47	3	Faure Walker et al. [6]
	0369294	4701335	-	-	12.6	Papanikolaou et al. [12]
Barete	0354574	4706216	130	65	-	Roberts and Michetti [14]
	0358438	4702072	239	49	9.1	Papanikolaou et al. [12]
	0358469	4702018	237	51	-	Faure Walker et al. [6]
	0358587	4701902	223	49	-	Faure Walker et al. [6]
	0360149	4700476	229	51	8.5	Roberts and Michetti [14]
	0362067	4699769	204	61	-	Roberts and Michetti [14]
Campo Felice	0369899	4677801	211	64	2.9	Morewood and Roberts [9]
	0371576	4676283	198	52	2.4	Morewood and Roberts [9]
	0372831	4675428	-	-	8.8	Papanikolaou et al. [12]
	0373014	4674776	212	59	2.8	Morewood and Roberts [9]
Campo Imperatore	0380389	4700028	-	-	-	Roberts and Michetti [14]
	0386404	4699825	-	-	6.7	Papanikolaou et al. [12]
	0386505	4700028	-	-	6	Roberts and Michetti [14]
	0394147	4698268	215	66	23.5	Faure Walker et al. [6]
	0398396	4690220	233	66	-	Faure Walker et al. [6]
	0398806	4696650	222	68	-	Faure Walker et al. [6]
Carsoli	0343943	4666185	-	-	7.1	Papanikolaou et al. [12]
	0344000	4666366	223	70	6	Roberts and Michetti [14]
	0346477	4662798	261	61	7	Roberts and Michetti [14]
	0346717	4662870	-	-	6.5	Papanikolaou et al. [12]
	0348513	4661740	-	-	3.5	Papanikolaou et al. [12]
	0348565	4661918	295	61	4	Roberts and Michetti [14]
	0350223	4660627	323	38	-	Roberts and Michetti [14]
Cassino	0400599	4605376	152	59	-	Roberts and Michetti [14]
	0406085	4598019	181	45	-	Roberts and Michetti [14]
	0409288	4593745	-	-	5	Papanikolaou et al. [12]
	0409548	4593686	225	53	6	Roberts and Michetti [14]
	0412218	4590832	248	41	4	Roberts and Michetti [14]
	0416659	4589252	277	52	-	Roberts and Michetti [14]
Fiamignano	0337173	4690531	175	39	4	Roberts and Michetti [14]
	0342018	4683819	231	65	-	Faure Walker et al. [6]
	0343375	4681877	-	-	19.4	Papanikolaou et al. [12]
	0345000	4682000	232	51	16.5	Roberts and Michetti [14]
	0350082	4679782	255	57	-	Faure Walker et al. [6]

	0352528	4676458	237	54	-	Faure Walker et al. [6]
	0353069	4675846	254	54	-	Faure Walker et al. [6]
	0355500	4674500	262	67	-	Roberts and Michetti [14]
Fucino	0372948	4671938	198	72	0.4	Morewood and Roberts [9]
	0372984	4671918	176	74	-	Morewood and Roberts [9]
	0373053	4671901	175	66	-	Morewood and Roberts [9]
	0373103	4671881	130	40	-	Morewood and Roberts [9]
	0373204	4671850	151	59	11.0	Morewood and Roberts [9]
	0373304	4671818	171	58	-	Morewood and Roberts [9]
	0373504	4673145	167	52	-	Roberts and Michetti [14]
	0373539	4671738	165	64	1.5+3.6=5.1	Morewood and Roberts [9]
	0373633	4671704	146	63	-	Morewood and Roberts [9]
	0375178	4670658	166	63	-	Morewood and Roberts [9]
	0375523	4670449	236	58	-	Morewood and Roberts [9]
	0375636	4670399	182	44	11.0	Morewood and Roberts [9]
	0376188	4667985	230	48	-	Morewood and Roberts [9]
	0376292	4667537	204	50	14.5	Morewood and Roberts [9]
	0376469	4667058	204	42	20.0	Morewood and Roberts [9]
	0376591	4666522	197	65	-	Morewood and Roberts [9]
	0377014	4665929	204	46	-	Roberts and Michetti [14]
	0377082	4665632	176	53	23.5	Morewood and Roberts [9]
	0377290	4664336	229	-	-	Morewood and Roberts [9]
	0377290	4664336	229	-	-	Morewood and Roberts [9]
	0377544	4664498	197	65	-	Roberts and Michetti [14]
	0389372	4647259	229	59	-	Morewood and Roberts [9]
	0389418	4647451	229	59	-	Roberts and Michetti [14]
	0393128	4644651	248	71	-	Morewood and Roberts [9]
	0393500	4645000	248	71	9	Roberts and Michetti [14]
	0394044	4644126	261	72	-	Morewood and Roberts [9]
	0394670	4643792	283	38	5.0	Morewood and Roberts [9]
	0395000	4643700	261	72	9	Roberts and Michetti [14]
Gioia Vecchio	0394595	4640092	-	-	9.9	Papanikolaou et al. [12]
	0394927	4640055	289	43	6	Roberts and Michetti [14]
Irpinia	0512000	4523200	109	60	-	Papanikolaou and Roberts [11]
	0515000	4521000	078	65	-	Papanikolaou and Roberts [11]
	0515232	4520580	-	-	9.8	Papanikolaou and Roberts [11]
	0517500	4518500	062	65	-	Papanikolaou and Roberts [11]
	0525300	4511000	336	56	-	Papanikolaou and Roberts [11]
	0527000	4509500	358	49	-	Papanikolaou and Roberts [11]
Irpinia Antithetic	0542557	4514780	-	-	4	Papanikolaou and Roberts [11]
Leonessa	0332371	4714421	053	58	6.5	Roberts and Michetti [14]
	0332381	4714191	-	-	5.7	Papanikolaou et al. [12]
Liri	0356964	4654004	150	53	6	Roberts and Michetti [14]

	0357047	4653842	-	-	7.7	Papanikolaou et al. [12]
	0361395	4651777	155	50	10	Roberts and Michetti [14]
	0364129	4648781	-	-	12	Papanikolaou et al. [12]
	0365852	4647538	212	71	20	Roberts and Michetti [14]
	0373946	4638900	-	-	14.7	Papanikolaou et al. [12]
	0374387	4638749	215	74	18	Roberts and Michetti [14]
	0376509	4634762	221	38	-	Roberts and Michetti [14]
	0379508	4633299	226	58	20	Roberts and Michetti [14]
	0385349	4626065	296	74	6	Roberts and Michetti [14]
	0393000	4620000	-	70	-	Roberts and Michetti [14]
Maiella	0422270	4660086	-	-	12.5	Roberts and Michetti [14]
	0425392	4642381	227	50	-	Faure Walker et al. [6]
Maratea	0558920	4443809	167	56	-	Papanikolaou and Roberts [11]
	0566197	4435333	233	55	-	Papanikolaou and Roberts [11]
	0562618	4429845	251	63	-	Papanikolaou and Roberts [11]
	0562700	4429519	-	-	7.8	Papanikolaou and Roberts [11]
	0562700	4429519	247	70	-	Papanikolaou [10]
	0564076	4425853	270	60	-	Papanikolaou and Roberts [11]
Mercure	0577628	4431226	164	61	-	Papanikolaou and Roberts [11]
	0581379	4430162	-	-	3	Papanikolaou and Roberts [11]
	0582833	4429747	192	60	-	Papanikolaou and Roberts [11]
	0582178	4429629	-	-	6.7	Papanikolaou and Roberts [11]
	0590742	4423481	252	64	-	Papanikolaou and Roberts [11]
Monte Alpi	0582282	4441140	261	75	-	Papanikolaou and Roberts [11]
	0583142	4438100	274	59	-	Papanikolaou and Roberts [11]
Montechristo	0381519	4697280	-	-	3.8	Papanikolaou et al. [12]
	0383799	4695998	240	52	4.7	Faure Walker et al. [6]
Parasano	0391986	4650700	224	56	-	Faure Walker et al. [5]
	0392144	4650643	237	57	8	Roberts and Michetti [14]
	0392776	4649992	-	-	5.2	Papanikolaou et al. [12]
Parasano Pescina Breach	0391544	4650707	224	60	9.7	Faure Walker et al. [5]
Pescina	0389531	4652123	-	-	5.5	Papanikolaou et al. [12]
	0390541	4651399	235	-	3.0	Faure Walker et al. [5]
Pescasseroli	0397490	4635700	158	68	-	Roberts and Michetti [14]
	0399361	4634061	206	-	4.9	Papanikolaou et al. [12]
	0399424	4633872	205	75	-	Faure Walker et al. [6]
	0401500	4631200	188	51	10	Roberts and Michetti [14]
	0403875	4627983	226	64	10	Roberts and Michetti [14]
	0403907	4627565	-	-	9.1	Papanikolaou et al. [12]
	0407351	4626281	241	9	10	Roberts and Michetti [14]
	0408903	4626329	249	27	5	Roberts and Michetti [14]
	0411513	4624397	262	32	3	Roberts and Michetti [14]

Pescocostanzo	0422364	4641081	216	50	-	Faure Walker et al. [6]
	0422905	4640424	-	-	3.0	Faure Walker et al. [6]
	0423282	4640149	222	42	-	Faure Walker et al. [6]
	0424055	4639203	238	52	2.4	Faure Walker et al. [6]
	0424380	4638982	256	51	-	Faure Walker et al. [6]
Pollino	0588419	4416598	175	60	-	Papanikolaou [10]
	0591153	4416303	176	60	-	Papanikolaou and Roberts [11]
	0604376	4413447	214	60	-	Papanikolaou and Roberts [11]
	0605223	4412845	-	-	5.4	Papanikolaou and Roberts [11]
	0605483	4412366	-	-	6	Papanikolaou and Roberts [11]
	0611287	4409150	-	-	3.5	Papanikolaou and Roberts [11]
Rieti segment	0323500	4711000	205	46	5	Roberts and Michetti [14]
Rieti	0328705	4701991	266	82	-	Roberts and Michetti [14]
	0332000	4695000	310	59	-	Roberts and Michetti [14]
Rocca Preturo	0389808	4673299	-	-	-	Faure Walker et al. [6]
	0392116	4672919	202	61	-	Faure Walker et al. [6]
	0392297	4672778	191	59	-	Faure Walker et al. [6]
	0392799	4672407	236	57	7	Faure Walker et al. [6]
	0393685	4671822	235	57	-	Faure Walker et al. [6]
	0394322	4671027	259	48	7	Faure Walker et al. [6]
San Gregorio	0528458	4502743	115	-	-	Papanikolaou and Roberts [11]
	0531997	4502634	187	-	-	Papanikolaou and Roberts [11]
	0532772	4502364	-	-	5.3	Papanikolaou and Roberts [11]
	0532772	4502364	193	50	-	Papanikolaou [10]
	0541359	4499943	232	-	-	Papanikolaou and Roberts [11]
San Gregorio (NNW dipping)	0535297	4499874	093	-	-	Papanikolaou and Roberts [11]
	0537554	4499123	015	-	-	Papanikolaou and Roberts [11]
San Sebastiano	0395300	4652521	226	65	-	Faure Walker et al. [6]
	0395728	4651053	254	63	-	Faure Walker et al. [6]
	0395887	4650748	238	62	-	Faure Walker et al. [6]
	0397378	4644678	-	-	5	Papanikolaou et al. [12]
	0397461	4644793	264	64	5	Roberts and Michetti [14]
Scurcola	0346556	4672543	150	49	-	Faure Walker et al. [6]
	0346579	4672869	176	52	5.5	Roberts and Michetti [14]
	0352977	4665855	-	-	7.4	Papanikolaou et al. [12]
	0353281	4665769	251	49	15	Roberts and Michetti [14]
	0357118	4661864	195	70	-	Faure Walker et al. [6]
	0360200	4660135	215	70	-	Faure Walker et al. [6]
	0360679	4660054	235	57	-	Faure Walker et al. [6]
	0362173	4658970	232	68	-	Roberts and Michetti [14]
	0365000	4656530	261	42	-	Roberts and Michetti [14]
	0368480	4650441	270	53	-	Roberts and Michetti [14]

Selladicorno	0340759	4701283	170	55	-	Roberts and Michetti [14]
	0346948	4694841	-	-	6.5	Papanikolaou et al. [12]
	0347049	4695166	223	57	6	Roberts and Michetti [14]
	0354950	4685754	310	45	1	Roberts and Michetti [14]
Sulmona	0403279	4670291	141	48	-	Roberts and Michetti [14]
	0407507	4664380	-	-	15.1	Papanikolaou et al. [12]
	0407610	4664659	209	52	20	Roberts and Michetti [14]
	0411154	4661141	-	-	18	Roberts and Michetti [14]
	0418410	4656207	258	38	-	Roberts and Michetti [14]
Trasacco	0379962	4644269	204	51	-	Roberts and Michetti [14]
	0381190	4642788	230	59	-	Faure Walker et al. [6]
	0381202	4642782	239	-	6.9	Papanikolaou et al. [12]
	0384594	4639570	283	42	15	Roberts and Michetti [14]
	0384718	4638512	233	55	15	Roberts and Michetti [14]
	0381168	4642841	228	70	8	Roberts and Michetti [14]
	0390122	4631873	280	50	7	Roberts and Michetti [14]
Tre Monti	0371435	4657592	147	71	-	Morewood and Roberts [9]
	0371711	4657722	194	64	3.6	Morewood and Roberts [9]
	0371927	4657790	165	63	-	Morewood and Roberts [9]
	0372101	4657811	156	63	-	Morewood and Roberts [9]
	0372259	4657849	136	57	2.4	Morewood and Roberts [9]
	0372487	4657965	200	66	-	Morewood and Roberts [9]
	0372829	4658132	181	64	-	Faure Walker et al. [6]
	0372830	4658092	146	71	-	Morewood and Roberts [9]
	0373050	4658264	162	60	-	Faure Walker et al. [6]
	0373055	4658241	146	68	2.4	Morewood and Roberts [9]
	0373507	4658301	143	52	-	Morewood and Roberts [9]
	0373801	4658399	164	61	-	Morewood and Roberts [9]
	0374007	4658699	159	67	-	Morewood and Roberts [9]
	0374306	4658955	134	52	1.8	Morewood and Roberts [9]
	0374515	4659161	126	41	-	Morewood and Roberts [9]
	0374955	4659087	158	53	0.7	Morewood and Roberts [9]
	0375777	4659491	204	-	-	Morewood and Roberts [9]
Val D'Agri Upper	0570741	4469864	-	-	6 (6+9 =15)	Papanikolaou and Roberts [11]
Val D'Agri Lower	0571296	4468174	-	-	9 (6+9 =15)	Papanikolaou and Roberts [11]
	0571296	4468174	172	66	-	Papanikolaou [10]
Val D'Agri	0554805	4484707	144	37	-	Papanikolaou and Roberts [11]
	0564873	4475358	188	58	-	Papanikolaou and Roberts [11]
	0570792	4469716	211	50	-	Papanikolaou and Roberts [11]
	0575947	4466001	251	64	-	Papanikolaou and Roberts [11]
	0582145	4463516	256	-	-	Papanikolaou and Roberts [11]

Vallo di Diano	0537182	4492810	-	-	3.3	Papanikolaou and Roberts [11]
	0538539	4492238	-	-	7.3	Papanikolaou and Roberts [11]
	0538539	4492238	190	57	-	Papanikolaou [10]
	0538722	4492225	188	55	-	Papanikolaou and Roberts [11]
	0538726	4491971	-	-	8	Papanikolaou and Roberts [11]
	0541066	4491239	209	62	-	Papanikolaou and Roberts [11]
	0545958	4479775	-	-	9.8	Papanikolaou and Roberts [11]
	0546264	4479056	240	55	-	Papanikolaou and Roberts [11]
	0552369	4471395	255	56	-	Papanikolaou and Roberts [11]
	0559487	4454453	293	45	-	Papanikolaou and Roberts [11]
Velino-Magnola	0356017	4680128	167	71		Morewood and Roberts [9]
	0362971	4668034	170	58	1.4	Morewood and Roberts [9]
	0364000	4667000	193	44	-	Roberts and Michetti [14]
	0364655	4666220	-	-	8.4	Faure Walker et al. [6]
	0368944	4665314	193	52	3.4	Morewood and Roberts [9]
	0371346	4664348	194	56	3.4	Morewood and Roberts [9]
	0371954	4664067	185	46	3.5	Morewood and Roberts [9]
	0374140	4664191	194	41	-	Roberts and Michetti [14]
	0375742	4663069	159	62	-	Morewood and Roberts [9]
Ventrino	0391544	4658336	215	49	-	Roberts and Michetti [14]
	0391986	4657816	245	58	2.7	Faure Walker et al. [6]
	0393070	4657467	255	56	-	Faure Walker et al. [6]

This data set does not include a few of the faults so in these cases throw-rates and slip vectors derived from other authors are used.

The displacement of a stratigraphic boundary, radiocarbon dated at 2020±80 BC, along the Carpino-Le Piano Fault suggests a throw-rate of 0.75 to 1.00 $\mathrm{mm\,yr^{-1}}$ near the centre of the fault that tends to zero towards the tips [3].

Topographic profiles across a displaced terrace show that the vertical slip rate (throw-rate) of the Laga Fault is 0.7-0.9mm/yr [7]. The average slip vector at the centre of the fault is $225^o \pm 5^o$ [1] and the plunge is estimated to be 65 ± 5^o (strike $140^o - 150^o$ and dip $60^o - 70^o$ [1]).

Observations on the Ocre Fault reveal a 3m high scarp [15].

For the Pettino Fault, a throw-rate of 0.47-0.86mm/yr was obtained from a 15-20m vertical offset of an alluvial terrace dated using stratigraphic correlation with the slope deposits in the area [7].

Based on the offset of a 36 ka unit, Cinque et al. [2] report throw-rates of 0.2-0.5 $\mathrm{mm\,yr^{-1}}$ on the Piana Volturno Fault [2].

The South Ufita Valley Fault has an estimated throw-rate of 0.2 $\mathrm{mm\,yr^{-1}}$ since the last glacial maximum [2] based on the offset of dated successions.

The centre of the Fucino basin fault is unexposed as it has been covered by lake beds. Here, we assign a throw of 8-18m, calculated using InSAR [13]. There is an additional error in the maximum throw for the InSAR measurements so as to allow for sedimentation on the lake beds. This error was estimated by extrapolating the sedimentation rate over 2000yrs in a near trench site [8].

We are not aware of any throw-rate measurements for the Apice, Avella, Benevento and Capitignano faults hence an estimate of 0.2mm/yr was derived by comparing them with faults within the area which have a similar length and known seismic activity. Whether there is a Late Pleistocene-Holocene

offset associated with the Piedmonte Matese, Gallo-Letino and Miranda-Pesche Faults could not be determined by field investigations hence these faults were assigned throw-rates of 0-0.2mm/yr; note this is the resolution above which we believe an offset can be seen and measured in the field (see 6 and 4).

Strain-rates, extension rates and mean topography within transects across the Apennines

Table 3 Strain rates in 5 x 90 km boxes.

X UTM	Y UTM	Principal strain-rate (/yr)	Strain-rate orthogonal to principal axis (/yr)	Extension rate (mm/yr)	Principal Angle (deg)	Mean Topography (m)
325512	4717956	0.00	0.00	0.00	-	865±85
329047	4714420	2.05±0.48E-09	-1.01±3.98E-10	0.18±0.04	036±3	870±93
332583	4710885	0.87±2.86E-10	-6.91±3.54E-10	0.01±0.03	105±5	898±88
336118	4707349	6.83±2.08E-10	-0.41±1.88E-10	0.06±0.02	083±3	916±84
339654	4703814	3.83±2.04E-10	4.30±6.30E-11	0.03±0.02	052±14	842±80
343189	4700278	5.14±1.00E-09	-4.38±8.27E-10	0.46±0.09	044±2	910±85
346725	4696743	1.32±0.26E-08	-0.41±2.16E-09	1.19±0.23	041±2	1003±89
350260	4693207	1.59±0.22E-08	0.15±1.74E-09	1.43±0.19	052±2	1046±53
353796	4689671	1.33±0.18E-08	-0.48±1.50E-09	1.20±0.16	034±2	991±55
357331	4686136	1.70±0.45E-08	1.39±4.21E-09	1.53±0.40	038±4	945±76
360867	4682600	1.38±0.22E-08	1.01±1.80E-09	1.25±0.20	034±2	987±85
364402	4679065	1.61±0.21E-08	9.52±1.70E-09	1.45±0.19	036±2	1050±80
367938	4675529	1.79±0.27E-08	0.66±2.13E-09	1.61±0.25	036±2	1206±93
371473	4671994	2.21±0.35E-08	-0.29±3.04E-0	1.99±0.31	037±6	1211±84
375009	4668458	2.15±0.23E-08	0.75±1.80E-09	1.93±0.21	040±2	1105±69
378544	4664923	$1.60^{+0.34}_{-0.27}$ E-08	$-0.60^{+2.39}_{-2.86}$E-09	$1.44^{+0.31}_{-0.24}$	040±3	1003±72
382080	4661387	$1.44^{+0.70}_{-0.31}$ E-08	$-0.79^{+2.61}_{-3.72}$E-09	$1.29^{+0.69}_{-0.28}$	042±2	886±74
385616	4657852	$1.21^{+1.06}_{-0.29}$ E-08	$-0.39^{+2.42}_{-4.09}$E-09	$1.09^{+0.95}_{-0.26}$	042±3	830±78
389151	4654316	$1.79^{+1.18}_{-0.24}$ E-08	$-0.94^{+1.99}_{-3.24}$E-09	$1.61^{+1.06}_{-0.22}$	042±3	686±78
392687	4650781	$3.41^{+0.83}_{-0.40}$ E-08	$0.68^{+3.41}_{-3.18}$E-09	$3.07^{+0.75}_{-0.36}$	044±2	799±78
396222	4647245	$2.62^{+0.49}_{-0.46}$ E-08	$-0.48^{+3.87}_{-3.99}$E-09	$2.35^{+0.44}_{-0.41}$	053±2	903±77
399758	4643710	1.20±0.29E-08	-0.90±2.44E-09	1.08±0.26	056±4	1048±89
403293	4640174	7.18±1.53E-09	-2.30±1.30E-09	0.65±0.14	044±2	1111±119
406829	4636638	8.50±1.63E-09	-1.50±1.30E-09	0.76±0.15	047±2	1099±122
410364	4633103	1.12±0.24E-08	-0.37±1.92E-09	1.00±0.21	046±2	970±110
413900	4629567	1.12±0.21E-08	-3.08±1.80E-09	1.01±0.18	038±2	912±104
417435	4626032	4.03±1.15E-09	-1.28±1.08E-09	0.36±0.10	056±3	986±109
420971	4622496	2.66±1.14E-10	-1.62±1.06E-10	0.02±0.01	018±4	958±86
424506	4618961	1.30±0.37E-09	-4.30±3.05E-10	0.12±0.03	026±3	856±73
428042	4615425	2.59±0.81E-09	-1.08±6.50E-10	0.23±0.07	037±3	806±81

X UTM	Y UTM	Principal strain-rate (/yr)	Strain-rate orthogonal to principal axis (/yr)	Extension rate (mm/yr)	Principal Angle (deg)	Mean Topography (m)
431577	4611890	3.29±0.92E-09	-0.37±7.35E-10	0.30±0.08	053±3	642±61
435113	4608354	$2.42^{+2.13}_{-0.63}$E-09	$-3.16^{+5.57}_{-6.79}$E-10	$0.22^{+0.19}_{-0.06}$	051±6	577±57
438649	4604819	$2.59^{+1.51}_{-0.63}$E-09	$-2.45^{+5.19}_{-4.14}$E-10	$0.23^{+0.14}_{-0.06}$	037±8	440±49
442184	4601283	$2.19^{+6.38}_{-1.71}$E-10	$-0.56^{+1.64}_{-2.09}$E-10	$0.02^{+0.06}_{-0.02}$	045±33	580±48
445720	4597748	$0.44^{+1.45}_{-0.17}$E-09	$-0.08^{+1.38}_{-3.79}$E-10	$0.04^{+0.13}_{-0.02}$	049±20	673±59
449255	4594212	$1.43^{+0.91}_{-0.52}$E-09	$-0.01^{+4.37}_{-5.34}$E-10	$0.13^{+0.08}_{-0.05}$	042±4	606±62
452791	4590676	2.61±0.57E-09	-1.76±4.70E-10	0.24±0.05	012±2	575±79
456326	4587141	$2.34^{+1.69}_{-0.76}$ E-09	$-1.28^{+6.17}_{-6.16}$ E-10	$0.21^{+0.15}_{-0.07}$	036±8	576±68
459862	4583605	$1.27^{+3.87}_{-0.31}$ E-09	$0.20^{+7.75}_{-2.47}$ E-10	$0.11^{+0.35}_{-0.03}$	059±8	556±64
463397	4580070	$0.67^{+3.24}_{-0.23}$ E-09	$-0.16^{+1.82}_{-6.78}$ E-10	$0.06^{+0.29}_{-0.02}$	078±9	540±73
466933	4576534	$0.01^{+1.41}_{-0.01}$ E-09	$-0.03^{+0.07}_{-3.15}$ E-10	$0.00^{+0.13}_{-0.00}$	068±6	413±62
470468	4572998	$0.01^{+1.61}_{-0.02}$ E-10	$-0.02^{+0.16}_{-9.36}$ E-11	$0.00^{+0.01}_{-0.00}$	117±47	410±55
474003	4569463	8.72±2.96E-10	-0.22±2.39E-10	0.08±0.03	001±4	389±52
477539	4565928	1.65±0.36E-09	-0.96±2.93E-10	0.15±0.03	031±3	440±53
481075	4562392	2.21±0.49E-09	1.17±3.95E-10	0.20±0.04	027±3	457±50
484610	4558857	2.47±0.63E-09	-1.09±4.97E-10	0.22±0.06	038±3	425±45
488146	4555321	1.72±0.37E-09	-1.43±2.98E-10	0.16±0.03	030±3	403±55
491682	4551786	8.61±2.09E-10	-0.53±1.74E-10	0.08±0.02	050±3	391±45
495217	4548250	9.30±3.62E-11	-3.03±3.16E-11	0.01±0.01	040±4	510±52
498753	4544714	0.00	0.00	0.00	-	464±36
502288	4541179	7.96±3.81E-11	-2.68±3.50E-11	0.01±0.00	020±4	446±33
505824	4537643	$1.25^{+0.54}_{-0.34}$ E-09	$-1.96^{+2.80}_{-2.80}$E-10	$0.11^{+0.05}_{-0.03}$	041±3	534±50
509359	4534108	$2.24^{+1.23}_{-0.48}$ E-09	$-0.63^{+3.81}_{-4.98}$E-10	$0.20^{+0.11}_{-0.04}$	049±3	608±47
512895	4530572	$7.76^{+6.27}_{-2.02}$ E-10	$-5.21^{+1.94}_{-5.31}$E-10	$0.07^{+0.06}_{-0.02}$	072±3	560±50
516430	4527037	$6.64^{+4.74}_{-3.12}$ E-10	$-7.10^{+4.31}_{-5.34}$E-10	$0.06^{+0.04}_{-0.03}$	077±7	577±50
519966	4523501	2.39±0.44E-09	-2.29±3.74E-10	0.22±0.04	051±2	613±69
523501	4519966	1.01±0.46E-09	-1.34±0.50E-09	0.09±0.04	092±4	533±67
527037	4516430	*1.73±3.46E-10*	-1.21±0.42E-09	0.02±0.03	158±4	454±50
530572	4512895	2.28±0.57E-10	-1.02±0.50E-10	0.02±0.01	007±3	490±66
534108	4509359	1.88±0.27E-10	-5.32±1.43E-10	0.17±0.02	167±3	489±71
537643	4505824	2.76±0.40E-09	-1.81±3.26E-10	0.25±0.04	026±2	477±53
541179	4502288	3.00±0.49E-09	-1.03±3.98E-10	0.27±0.04	035±2	597±54
544715	4498753	1.55±0.49E-10	-3.95±8.01E-10	0.14±0.04	179±8	631±55
548250	4495217	3.33±1.42E-09	-1.14±1.18E-09	0.30±0.13	064±4	631±50
551786	4491682	5.03±0.92E-09	-2.54±7.45E-10	0.45±0.08	064±2	735±50
555321	4488146	3.83±1.31E-09	0.05±1.05E-09	0.35±0.12	068±4	680±36
558857	4484610	2.93±0.85E-09	1.05±5.52E-10	0.27±0.08	043±5	795±48
562392	4481075	4.62±1.59E-09	6.40±9.53E-10	0.42±0.14	015±6	953±68
565928	4477539	4.30±0.98E-09	2.11±7.74E-10	0.39±0.09	042±4	856±59

X UTM	Y UTM	Principal strain-rate (/yr)	Strain-rate orthogonal to principal axis (/yr)	Extension rate (mm/yr)	Principal Angle (deg)	Mean Topography (m)
569463	4474004	6.71±2.26E-09	-0.22±1.82E-09	0.60±0.20	037±4	717±55
572999	4470468	6.23±1.53E-09	-0.05±1.25E-09	0.56±0.14	025±3	663±61
576534	4466933	3.44±0.83E-09	-2.23±6.80E-10	0.31±0.08	056±3	762±63
580070	4463397	1.31±0.30E-09	-0.93±2.63E-10	0.12±0.03	035±2	694±59
583605	4459862	1.97±0.60E-09	-0.82±4.83E-10	0.18±0.06	037±3	677±63
587141	4456326	4.73±0.84E-09	-8.33±6.91E-10	0.43±0.08	081±2	656±76
590676	4452791	2.78±0.51E-09	1.71±4.33E-10	0.25±0.05	073±2	529±66
594212	4449255	1.02±0.30E-09	1.32±2.71E-10	0.09±0.03	084±3	527±73
597748	4445720	1.89±0.35E-09	-0.33±2.90E-10	0.17±0.03	019±2	496±64
601283	4442184	2.05±0.56E-09	-0.73±4.61E-10	0.19±0.05	029±3	508±51
604819	4438649	8.17±2.16E-10	-1.00±1.80E-10	0.07±0.02	050±3	406±43
608354	4435113	3.14±1.57E-10	0.19±1.47E-10	0.03±0.01	017±8	564±79
611890	4431577	1.17±0.41E-09	-0.02±3.32E-10	0.11±0.04	011±4	723±98
615425	4428042	2.02±0.50E-09	-0.17±4.07E-10	0.18±0.04	021±3	743±107
618961	4424506	2.27±0.55E-09	-0.79±4.54E-10	0.20±0.05	040±3	714±110
622496	4420971	9.49±4.84E-10	-2.56±4.54E-10	0.09±0.04	053±4	383±79

38 Table 4 Strain-rates in 20 x 90 km boxes

X UTM	Y UTM	Principal strain-rate (/yr)	Strain-rate orthogonal to principal axis (/yr)	Extension rate (mm/yr)	Principal Angle (deg)	Mean Topography (m)
334350	4709117	5.91±1.46E-10	0.11±1.31E-10	0.05±0.01	055±5	882±43
348492	4694975	1.17±0.10E-08	-1.09±8.10E-10	1.05±0.09	043±1	987±37
362635	4680833	1.62±0.15E-08	1.01±1.34E-09	1.46±0.13	034±2	105±43
376777	4666690	$1.85^{+0.25}_{-0.14}$E-08	$-0.22^{+1.25}_{-1.47}$E-09	$1.66^{+0.22}_{-0.13}$	040±2	105±39
390919	4652548	$2.24^{+0.75}_{-0.18}$E-08	$-0.13^{+1.47}_{-1.88}$E-09	$2.02^{+0.68}_{-0.16}$	046±1	804±39
405061	4638406	9.64±1.09E-09	-1.20±0.89E-09	0.87±0.10	049±2	106±56
419203	4624264	4.06±0.58E-09	-1.09±0.51E-09	0.37±0.05	041±2	928±47
433345	4610122	$2.65^{+0.98}_{-0.37}$E-09	$-0.98^{+3.01}_{-3.33}$E-10	$0.24^{+0.09}_{-0.03}$	045±2	617±34
447487	4595980	$1.04^{+0.74}_{-0.19}$E-09	$0.70^{+1.52}_{-1.34}$E-10	$0.09^{+0.07}_{-0.02}$	027±4	609±32
461630	4581838	$0.99^{+2.09}_{-0.19}$E-09	$0.55^{+4.36}_{-1.49}$E-10	$0.09^{+0.19}_{-0.02}$	054±4	521±34
475772	4567695	$1.14^{+0.17}_{-0.16}$E-09	$0.42^{+1.42}_{-1.31}$E-10	$0.10^{+0.02}_{-0.01}$	024±2	424±26
489914	4553553	1.27±0.19E-09	-0.65±1.51E-10	0.11±0.02	037±2	432±25
504056	4539411	$8.83^{+3.77}_{-1.46}$E-10	$-0.61^{+1.17}_{-1.65}$E-10	$0.08^{+0.03}_{-0.01}$	045±2	513±22
518198	4525269	$1.06^{+0.22}_{-0.18}$E-09	$-5.51^{+1.67}_{-2.62}$E-10	0.10±0.02	072±3	571±30
532340	4511127	1.04±0.13E-09	-2.91±1.20E-10	0.09±0.01	002±1	478±20
546482	4496985	2.74±0.51E-09	0.16±4.24E-10	0.25±0.05	053±3	648±27
560624	4482843	3.54±0.51E-09	6.34±3.56E-10	0.32±0.05	042±4	821±29

X UTM	Y UTM	Principal strain-rate (/yr)	Strain-rate orthogonal to principal axis (/yr)	Extension rate (mm/yr)	Principal Angle (deg)	Mean Topography (m)
574767	4468701	4.26±0.71E-09	0.14±5.66E-10	0.38±0.06	036±2	709±30
588909	4454558	2.41±0.27E-09	0.60±2.24E-10	0.22±0.02	073±2	597±35
603051	4440416	1.23±0.18E-09	-0.03±1.45E-10	0.11±0.02	028±2	494±31
617193	4426274	1.49±0.23E-09	0.18±1.87E-10	0.13±0.02	037±2	640±51

[1] Boncio, P., Lavecchia, G., Milana, G., Rozzi, B., 2004. Seismogenesis in central Apennines, Italy: an integrated analysis of minor earthquake sequences and structural data in the Amatrice-Campotosto area. Annals of Geophysics 47 (6), 1723–1740.

[2] Cinque, A., Ascione, A., Caiazzo, 2000. Distribuzione spazio-temporale e caratterizzazione della fagliazione quaternaria in Appennino meridionaleDistribuzione spazio-temporale e caratterizzazione della fagliazione quaternaria in Appennino meridionale. CNR-Gruppo Nazionale per la Difesa dai Terremoti - Roma, pp. 203–218.

[3] Di Bucci, D., Corrado, S., Naso, G., 2002. Active faults at the boundary between central and southern Apennines (Isernia, Italy). Tectonophysics 359 (47-63).

[4] Faure Walker, J. P., 2010. Mechanics of continental extension from Quaternary strain field in the Italian Apennines. Ph.D. thesis, University College London.

[5] Faure Walker, J. P., Roberts, G. P., Cowie, P. A., Papanikolaou, I., Michetti, A. M., Sammonds, P., Phillips, R., 2009. Horizontal strain-rates and throw-rates across breached relay-zones, central Italy: implications for the preservation of throw deficits at points of normal fault linkage. Journal of Structural Geology 31 (doi:10.1016/j.jsg.2009.06.01), 1145–1160.

[6] Faure Walker, J. P., Roberts, G. P., Sammonds, P., Cowie, P. A. C., 2010. Comparison of earthquake strains over 100 and 10,000 year timescales: insights into variability in the seismic cycle in the central Apennines, Italy. Journal of Geophysical Research 115 (B10418), doi:10.1029/2009JB006462.

[7] Galadini, F., Galli, P., 2000. Active tectonics in the Central Apennines (Italy) - input data for seismic hazard assessment. Natural Hazards 22, 225–270.

[8] Michetti, A. M., Brunamonte, F., Serva, L., Vittori, E., 1996. Trench investigations of the 1915 Fucino earthquake fault scarps (Abruzzo, Central Italy): geological evidence of large historical events. Journal of Geophysical Research 101 (B3), 5921–5936.

[9] Morewood, N., Roberts, G. P., 2000. The geometry, kinematics and rates of deformation within an en echelon normal fault boundary, central Italy. Journal of Structural Geology 22, 1027–1047.

[10] Papanikolaou, I., 2005. Ph.D. thesis, University College London.

[11] Papanikolaou, I. D., Roberts, G. P., 2007. Geometry, kinematics and deformation rates along the active normal fault system in the southern Apennines : Implications for fault growth. Journal of Structural Geology 29, 166–188.

[12] Papanikolaou, I. D., Roberts, G. P., Michetti, A. M., 2005. Fault scarps and deformation rates in Lazio-Abruzzo, Central Italy: Comparison between geological fault slip-rate and GPS data. Tectonophysics 408, 147–176.

[13] Pizzi, A., Pugliese, G., 2004. InSAR-DEM analyses integrated with geologic field methods for the study of long-term seismogenic fault behavior: Applications in the axial zone of the central Apennines (Italy). Journal of Seismology 8, 313–329.

[14] Roberts, G. P., Michetti, A. M., 2004. Spatial and temporal variations in growth rates along active normal fault systems: an example from the Lazio-Abruzzo Apennines, central Italy. Journal of Structural Geology 26, 339–376.

[15] Salvi, S., Cinti, F. R., Collini, L., D'Addezio, G., Doumaz, F., Pettinelli, E., 2003. Investigation of the active Celano-L'Aquila Fault System, Abruzzi (central Apennines, Italy) with combined ground penetrating radar and palaeoseismic trenching. Geophysical Journal International 155, 805–818.